IEEE Access
Multidisciplinary | Rapid Review | Open Access Journal

Received November 29, 2020, accepted December 13, 2020, date of publication December 18, 2020,
date of current version January 11, 2021.

Digital Object Identifier 10.1109/ACCESS.2020.3045716

Challenges Faced by Electric Vehicle Motors and Their Solutions

ZHIKUN WANG[1], TZE WOOD CHING[2], (Senior Member, IEEE), SHAOJIA HUANG[3], HONGTAO WANG[1], (Member, IEEE), AND TAO XU[1]

[1]Faculty of Intelligent Manufacturing, Wuyi University, Jiangmen 529020, China
[2]Faculty of Science and Technology, University of Macau, Macau, China
[3]Faculty of Mechanical Engineering, Zhuhai College of Jilin University, Zhuhai 519041, China

Corresponding authors: Tze Wood Ching (twching@ieee.org) and Tao Xu (wanxiao0756@gmail.com)

This work was supported in part by the Startup Funds for Scientific Research of High-Level Talents of Wuyi University under Grant 2019AL020, in part by the Jiangmen Science and Technology Project under Grant 2020030102220005387, in part by the Off Campus Practice Teaching Base for College Students of Zhuhai College of Jilin University under Grant ZLG20180703, in part by the Special Projects in Key Fields Supported by the Technology Development Project of Guangdong Province under Grant 2020ZDZX3018, and in part by the Science Foundation for Young Teachers of Wuyi University under Grant 2018td01.

ABSTRACT This paper reviews motor techniques for reducing the cost of electric vehicles (EVs) and improving their range. In recent years, environmental issues, energy crises and the greenhouse effect have urged the popularization of clean energy EVs. In order to achieve this goal, it is necessary to overcome technical difficulties in vehicle cost and range. As a key component of an EV, the motor occupies a large proportion of the overall vehicle cost, and its efficiency directly affects the mileage. In this context, this article discusses the merits and challenges of three mainstream EV motors: permanent magnet synchronous motor (PMSM), induction motor (IM), and switched reluctance motor (SRM) in terms of vehicle cost and range. Then this paper compares the advanced techniques of these motors in terms of topology, material applications and control strategies. Finally, the development trends and opportunities of the three motors in EVs are predicted.

INDEX TERMS Electric vehicles, EV motor, control strategy, motor topology development.

I. INTRODUCTION

In the past ten years, environmental problems caused by many greenhouse gas emissions have become increasingly serious, which has promoted countries to pay more attention to energy conservation and emission reduction. Transportation is one of the largest contributors of greenhouse gas emissions: it accounts for approximately 27% of the total emissions [1]. However, fuel vehicles are still the main component of the transportation system [2]. Due to the development of batteries, and the desire to reduce greenhouse gas emissions and improve urban air quality, the electric vehicle (EV) manufacturing industry has begun to receive attention from governments. Compared to internal combustion engine vehicles (ICEVs), the benefits of EVs include zero exhaust emissions, higher efficiency, and the vast potential for reducing greenhouse gas emissions combined with the low-carbon power sector. In this context, many countries have successively announced the goal of achieving 100% zero-emission vehicles or phasing out ICEVs by 2050, and proposed incentives for EV purchase and production to support the development of the EV industry. However, in 2019, the number of available EVs was 7.2 million, which is only approximately 1% of the global car inventory [3]. Therefore, the popularization of EVs still has a long way to go.

According to the survey results of [4], [5], the main obstacle to the use of the EV is the concern about mileage. Drivers do not need to worry about the availability of gas stations when using ICEVs but need to plan their trips to avoid insufficient power before reaching the charging station. On the other hand, the higher expenditure for the purchase of EVs also reduces the adoption of EVs. Considering policy subsidies, the total cost of EVs is slightly lower than that of ICEVs [6]. However, government subsidies for supporting EV purchases are short-lived. When sales increase by a certain amount, the subsidies will be canceled. In the absence of subsidies, the cost of EVs is difficult to compete with ICEVs with current EV techniques and manufacturing scale and thus hindering the continued growth of EV sales. The main reasons that hinder the popularization of EVs can be

The associate editor coordinating the review of this manuscript and approving it for publication was Jun Shen.

attributed to short mileage and the high cost of EVs. These problems are closely related to the performance and cost of the motor system. The mileage is directly affected by the efficiency of the motor and power/torque density, and the cost of the motor is second only to the cost of the battery [7]. However, as far as the author knows, there is currently no published article comprehensively discussing motor design and control methods for low-cost, long-range EVs.

In this context, this article reviews the challenges faced by different EV motors to achieve low-cost, long-range EVs, and current solutions to overcome them. Next, the second part of the article investigates the merits and drawbacks of various current EV motors including PMSMs, IMs and SRMs, and lists their shortcomings that hinder the popularization of EVs. The third to the fifth part of the article sequentially compares the defect solutions of the three EV motors.

II. CURRENT CHALLENGES OF EV MOTORS

We investigate the EV market from 2010 to 2020 and show motors used in some EV models in Table 1. We conclude that the motors that are currently installed in EV propulsion systems mainly consists of the PMSM, IM, and SRM. Among them, the PMSM has become the first choice of EV manufacturers due to the high torque and high power density enabled by high-energy-density PMs (neodymium Fe boron (NdFeB) and samarium cobalt (SmCo)) [8]–[11]. The PMSM is divided into the internal-PMSM and the surface-PMSM. With the same size, the overload capacity of the internal-PMSM is better [9], so the internal-PMSM is more common in EVs. Because the high-energy-density PM is affected by low yield and is non-renewable and geopolitical, its cost is at least twice than the total cost of other raw materials of electric motors [12]. Therefore, techniques that can reduce PM costs without substantially sacrificing performance are urgent and important for the EV industry. The permanent magnet assisted synchronous reluctance motor (PMasyRM) and spoke-type motor are low-cost solutions for PM motors.

Among PM-free motors, the IM has successfully penetrated the EV market with its mature techniques and low-cost advantages (Table 1). However, due to the limitation of its structure, the efficiency performance of the IM is worse than other motors [11], [13], which is not conducive to EV mileage. It is foreseeable that with the development of other motor techniques, the cost advantage of mature IM technology will be gradually reduced. For example, the SRM with the lowest material cost is receiving an increasing amount of attention [12]. To achieve the same output power (30kW), the material cost of SRM is approximately half of the PMSM (NdFeB) and less than 80% of that of the IM. However, considering the shortcomings of low torque density, high torque ripple, and high noise, few EVs currently use SRM (Table 1).

In addition, because the regenerative braking technique can recover electrical energy for long mileage, this technique is becoming increasingly important for EVs. Improving the motor-related performance to increase the energy recovered by regenerative braking has become a new challenge for EV motors. According to the analysis of [14]–[17], the energy recovered by braking is proportional to the torque and motor efficiency, and the effect of regenerative braking is best in the constant power region close to the base speed. Therefore, to improve the energy recovery effect of regenerative braking, the EV motor needs to have as wide a constant power range as possible in addition to the highest efficiency. Based on motor design research [18]–[21], it can be seen that the PMSM with its high efficiency and wide constant power range is the most suitable EV motor for regenerative braking. The energy recovery rate of the IM is affected by low efficiency, which also reduces the output power, and shortens the constant power range. Although the SRM has a wide speed range due to its excellent high-temperature resistance and reliable mechanical structure, its poor torque capacity limits the energy recovery effect.

The advantages of PM motors are high efficiency, high torque density, and suitability for long-range EVs. The expensive cost of the PM is a challenge to overcome. In PM-free

TABLE 1. Example of EVs on the market from 2010 to 2020, including their model, motor categories, and power.

EV model	Power(kW)	Motor	Year
Mahindra e2o Plus	19-30	IM	2016
Renault Kangoo ZE	44	PMSM	2011
Mitsubishi i-MiEV	47	PM	2010
Volkswagen E-up	60	PMSM	2019
Renault Zoe	65	PMSM	2012
LandRover	70	SRM	2013
Renault Fluence Z.E.	70	PMSM	2012
Nissan Leaf	80	PMSM	2010
BJEV EC5	80	PMSM	2019
Hyundai Ioniq Electric	88	PMSM	2016
Hyundai Kona	88-150	PMSM	2018
BYD E6	90	PMSM	2014
BMW i3	125	PMSM	2013
Xpeng G3	139	PMSM	2018
Mercedes-Benz EQC	150*2	IM	2019
BJEV EU5	160	PMSM	2018
Tesla Model X	193-375	IM	2015
Tesla Model 3	211-340	PMSM	2020
Tesla Model S	235-568	IM	2012
NIO EC6	320	PMSM	2020
NIO ES6	320	PMSM	2020

TABLE 2. Price and properties of PM materials [22].

Property	Alnico	Ferrites (ceramic)	Samarium cobalt	Neodymium
Remanence (Br, T)	0.7-1.28	0.23-0.41	0.83-1.16	1.00-1.41
Coercitive force (Hc, kA/m)	37-143	50-290	480-840	760-1030
Max. energy product, $(BH)_{max}$, kJ/m^3	10.7-71.6	8.35-31.8	130-240	220-336
Electric resistivity, ρ, Ω cm	$(50\text{-}75)*10^{-6}$	10^{-6}	$(53\text{-}86)*10^{-6}$	$160*10^{-6}$
Max. service temperature, T_{max}, °C	450–550	800	300-350	150
Density, d, g/cm^3	6.8-7.3	4.9	8.4	7.4
Price, USD/kg	58	7.1	100	75

motors, the IM cost and torque density are moderate whereas its low efficiency is a disadvantage. The cost advantage of the SRM is obvious, but the torque density is low, and shortcomings of torque ripple and noise affect the application of EVs. Next, we will introduce and compare the latest techniques that can compensate for the shortcomings of these motors.

III. MAIN DEFECTS OF PMSM AND COMPENSATION METHODS

A. ALTERNATIVES TO EXPENSIVE PM MATERIALS

Due to the low yield of rare earth elements and non-renewable property, the rare earth PM is expensive. Therefore, the application of low-cost rare earth-free PM in motors has gradually attracted attention. Currently, the PM material that is employed to manufacture motors can be classified into four types: AlNiCo, ferrite, NdFeB, and SmCo, of which the latter two are rare earth-containing materials [12], [13], [22].

Rare earth elements, such as Nd and Sm, can be fabricated into high-energy-density PMs. However, the reserves of these two elements are scarce and the distribution is not concentrated in nature, which leads to high prices and an unstable supply. Currently, the high-energy-density PM is mainly divided into NdFeB-based PMs and SmCo-based PMs, in which the NdFeB-based PM is the main choice for PM motors because of their high coercivity [12]. Magnets with low energy density and low coercivity are unable to meet the needs of high-performance EVs, but their low cost is very attractive to low- and medium-performance EVs. Table 2 shows the price and properties of PM materials [22].

Compared with rare earth materials, rare earth-free materials are mainly poor in coercivity and maximum energy products, which affects the anti-demagnetization ability and torque density, respectively, of the motor. Currently, the magnet market of rare earth-free magnets is mainly occupied by AlNiCo and ferrite. The AlNiCo magnets are mainly composed of nickel (Ni), Co, aluminum (Al), and Fe without rare earth elements. These magnets can provide the same high remanence as SmCo PMs but are easily demagnetized due to their very low coercivity [12], [13], [22]. In addition, since the Co content accounts for approximately 20% of the total composition, the price advantage of AlNiCo is not obvious (Table 2). However, the low coercivity contributes an excellent field weakening ability, which can achieve a higher speed. This high speed produces a low torque that can generate the same power, which conserves space for the EV. Compared with the traditional flux-weakening control mode that requires continuous current to change the magnet remanence [23], changing the magnetization level of AlNiCo-PM requires only a simply short current pulse to be injected into the stator [24]. Thus, the copper loss can be reduced and the motor efficiency can be increased. The motor that uses this variable magnetic flux characteristic is referred to a flux memory motor [24]. In [25]–[27], this characteristic is combined with other topology techniques to improve the performance of the motor. For example, in [27], a new type of memory motor which incorporates both AlNiCo-PM and NdFeB-PM is proposed, namely the stator-PM doubly salient flux memory (DSFM) motor. This motor can not only retain high torque density due to NdFeB-PM but also offer efficient air-gap flux control due to the AlNiCo-PM.

Ferrite magnets which consist of Fe oxide are the most popular rare earth-free PMs for PM motors due to their very low cost, although its coercivity and energy density are not high. Currently, to compensate for the shortcomings of low coercivity and energy density, ferrite PM motors have been extensively investigated and are considered to be a feasible direction to solve the high cost of PM motors in the future [13], [28]. We introduce the advanced technology of ferrite PM motors in detail in the next part.

B. FERRITE PM MOTOR TECHNOLOGY

Due to the extremely low raw material cost, ferrite PM is a feasible solution for reducing the cost of EV. Given the shortcomings of relatively low energy density and coercivity, many new techniques related to motor topology are proposed, among which three kinds of topologies are employed, namely the spoke type PM motor, axial flux PM motor, and PM-assisted synchronous reluctance motor [29]–[36].

1) PM-ASSISTED SYNCHRONOUS RELUCTANCE MOTOR (PMASYNRM)

The PMasynRM is similar to the IPSM whereas the difference is the ratio of the reluctance torque and permanent magnet torque to the total torque. The PMasyRM improves the reluctance torque by optimizing the design of rotor barriers, segments, and ribs, which can partially compensate for the decrease in torque performance caused by the reduction in the rare earth PM. Therefore, this topology is suitable for combining with ferrite PM as a low-cost solution with a small sacrifice in torque performance [32], [33], [35]–[37]. FIGURE 1 and FIGURE 2 show the structure of conventional synchronous reluctance motors without PM and PMasynRM motors, respectively [33], [38]. Currently, the torque/PM cost of the ferrite PMasyRM can reach 15.6 Nm/USD whereas the cost of the mixed design of ferrite and NdFeB can

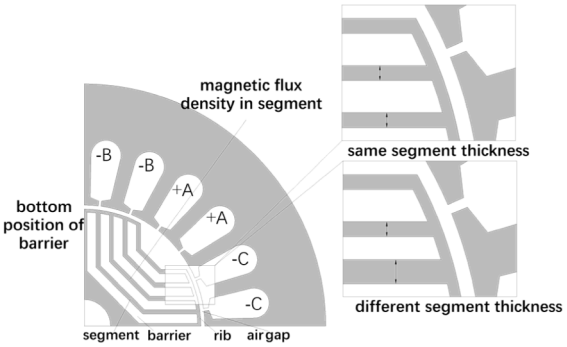

FIGURE 1. Rotor-/stator-structure of conventional synchronous reluctance motors without PM [38].

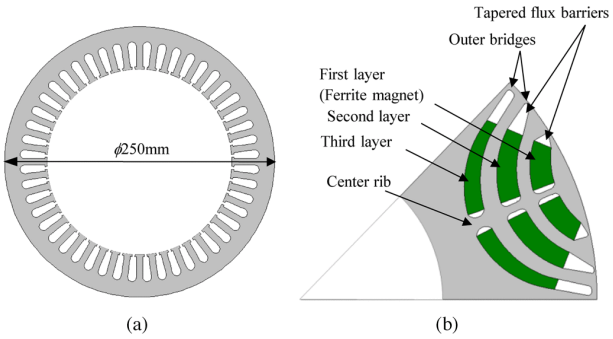

FIGURE 2. Structure of PMASynRM motor [33]. (a) stator and (b) rotor.

reach 17.64 Nm/USD [37], which is more than four times the cost of the PMSM in the Toyota PRIUS 2010 [39]. However, the low coercivity of ferrite must be considered.

To avoid demagnetization, the ferrite magnets do not fill each layer, rather than leave space on both sides of the magnetic pole as flux barriers showed in FIGURE 2 to hinder the magnetomotive force (MMF) generated by the stator. However, in the worst conditions (critical temperature is −40 °C, 1.5 times the maximum current), the demagnetization rate for the ferrite magnet still exceeds 10% [35], although there are flux barriers. To solve this problem, the authors of [35], [36] proposed a tapered flux barrier that is designed to disperse the flux, which reduces demagnetization. With this design, the demagnetization rate in the worst condition is reduced to less than 10%. FIGURE 3 shows the flux density vectors of the second layer tapered flux barrier and common flux barrier in the worst condition. Comparing the dotted portion of FIGURE 3 (a) and FIGURE 3 (b), it can be seen that the tapered magnetic barrier makes the magnetic flux more dispersed.

2) SPOKE TYPE PM MOTOR

The spoke type PM motor can hold more volume of the PM compared to other PM motors, and can effectively use the reluctance torque by optimizing the rotor design [40]. Therefore, the spoke type motor is suitable for combining with ferrite as a solution of low-cost and high-performance PM motors [34], [41]. FIGURE 4 shows the cross-section

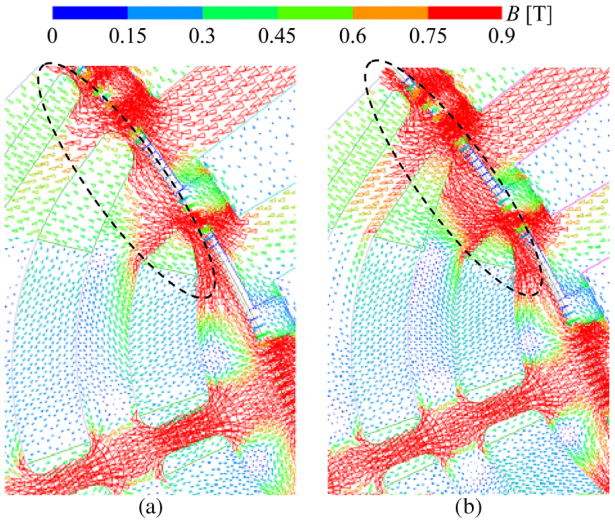

FIGURE 3. Flux density vectors of second-layer tapered flux barrier and common flux barrier in the worst conditions (1.5 times the maximum current, −40 °C) [35]. (a) Common flux barrier. (b) Second layer tapered flux barrier.

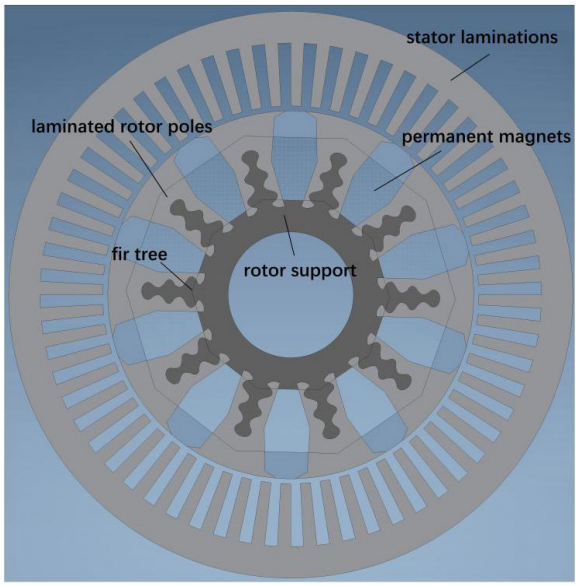

FIGURE 4. Cross-section schematic of spoke type ferrite motor design [48].

of the spoke-type ferrite motor. Currently, the spoke type motor of ferrite PM can achieve the same torque density as the rare earth PMSM [34]. However, considering the demagnetization of ferrite PM and the stress of the magnet on the rotor [42], [43], the extra space is not completely utilized to increase the ferrite PM volume to increase the torque density but is employed as an air barrier to enhance the ability of anti-demagnetization. For example, in [34], due to the large volume of the spoke type structure, air gaps can be installed on the top and bottom of the permanent magnet as a magnetic flux barrier, which prevents the permanent magnet from demagnetizing in the worst conditions (1.6 times the rated peak current, −40 °C). FIGURE 5 shows the field

TABLE 3. PM motor topology technology performance comparison.

Effectiveness	Torque/PM total cost (Nm/USD)	Torque density (Nm/L)	Power density (kW/L)	Maximum torque (Nm)	Power (kW)	Topology	Refe rence
90	3.53 (NdFeB)	33.4	4.8	207	60	PMSM（Toyota Prius 2010）	[40]
91	13.1 (ferrite)	35.3	10.24	208.8	60.5	Axial double stator spoke-type	[61]
93	13 (ferrite)	35.3	10.24	208.8	60.5	double stator spoke-type	
No mention	9.05 (ferrite)	36	5.68	320	50	Axial double stator	[30]
92	3.79 (NdFeB and ferrite)	53.9	25.7	169.5	81.5	PMasyRM	[38]
No mention	15.6-17.64 (ferrite)	40.8-44	24.9	128.3-138.3	78.4		
90 (estimated)	0.85 (NdFeB)	72.5	9.1	231	29	Axial double stator	[62]
90 (estimated)	12.14 (ferrite)	33.14	4.1	153	19		
90.2	1.565 (NdFeB)	83.2	24.79	207.8	61	Spoke-type	[14]
89.6	15.15 (ferrite)	47.5	13.9	187.2	55		

The PM cost used is calculated based on the PM cost of Table II, the density of NdFeB (7 g/cm3), and the PM density of ferrite (5.1 g/cm3)

strength of a PM (white frame) with bottom and top air gaps during a three-phase short circuit.

3) AXIAL FLUX PM MOTOR

Compared with the radial flux permanent magnet synchronous motor [44]–[47], the axial flux permanent magnet synchronous motor has the advantages of a compact axial structure and high torque density, so it may be a direction to realize the low-cost PM motor. In [29], [31], researchers proposed the high torque density axial magnetic flux topology with low-cost ferrite PM, and thus the torque/PM-cost reached 9.05 Nm/USD and 13.31 Nm/USD respectively. In [29], a ferrite PM axial gap motor with a segmented rotor structure was proposed. This design can make effective use of reluctance torque to compensate for lower magnet torque, and, by increasing the number of concentrated winding stator slots to disperse the magnetic flux, the problem of ferrite demagnetization is alleviated. In [31], aimed at Toyota Prius (2010)'s motor, the topology design of the ferrite PM axial flux motor with a dual stator is proposed.

4) FERRITE PM TOPOLOGY PERFORMANCE AND COST COMPARISON

Table 3 compares the torque/PM cost and torque density of the previously described PM motor design. The ferrite PM motor that combines the advantages of the topology can achieve the same torque density as the PMSM Toyota Prius 2010 and significantly improve the torque cost ratio. It can be predicted that the competitiveness of rare earth-free PM motors with a maximum torque of less than 200 Nm will become stronger with the development of technology. However, the problem of ferrite demagnetization prevents further improvement in torque performance. For cost-insensitive high-performance EVs, rare earth PM combined with a mature PMSM structure will be the main choice in the future.

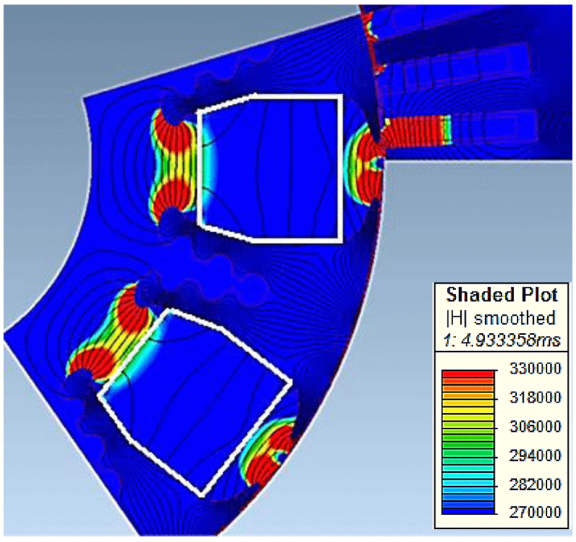

FIGURE 5. Field strength (in amperes per meter) distribution during the three-phase short circuit [34].

IV. MAIN DEFECTS OF IM AND THE CURRENT COMPENSATION METHOD

The IM has successfully penetrated the EV market with its mature techniques and low-cost advantages brought by no PM (Table 1). With the development of other motor techniques, the cost advantage of mature IM technology will be gradually reduced. Tesla, which is the vane of the EV industry, also began to use PM motors instead of IMs in new products [49]. The speed range of IMs is wider and easier to achieve than permanent magnet motors because the magnetic field of the IM is provided entirely by electromagnetic induction. IMs do not need to consider PM demagnetization when changing the speed. However, the absence of high-energy-density PMs cause IMs to have a low torque performance. In addition, excitation current through the rotor windings or bars generates loss which causes reduced

efficiency. Therefore, the low efficiency limits the application of IMs in EVs, which have high requirements for space utilization and battery life. To compensate for this shortcoming, many control strategies and topology technologies have been proposed, and they will be introduced in this chapter.

A. METHODS TO IMPROVE IM EFFICIENCY

Improving the efficiency of IMs can be achieved by reducing loss and increasing the power factor. The losses can be divided into resistance losses, core losses, and stray losses, of which resistance losses and core losses account for the largest proportion of total losses [50]. In terms of resistance losses, since the operation of IMs uses the principle of electromagnetic induction, the resistance losses caused by the stator excitation current and rotor induction current cannot be completely eliminated. The method of reducing resistance losses is mainly realized by improving conductivity and conductor current density [51], [52].

1) REDUCE MATERIAL LOSS

IM rotor conductor materials can be divided into Al, copper, and alloys. Among them, copper's electrical conductivity is nearly 60% higher than Al, which is suitable for a high-efficiency motor. The alloy is utilized to increase the yield strength and has no positive effect on the electrical conductivity once it is added [53]. Considering the cost, most rotors were composed of Al. In the past ten years, the copper casting process was not mature enough, mainly because no durable mold could withstand the high temperature of copper casting [54], which consequently leads to excessive production costs of copper rotors. With the development of copper casting technology, the cost and quality of copper rotors have met the requirements of EV mass production [55]–[58]. In [59], the efficiency advantage of the copper rotor is demonstrated and the methods for overcoming the main difficulties in casting copper are reviewed. Moreover, it is mentioned that a copper rotor production system with large-scale production capacity exists. Although the copper rotor is more expensive, its high conductivity can lead to a reduction in the size of the motor and cost of the casing. Therefore, there is a trade-off point between rising costs and falling costs. To identify the trade-off point, [56] proposes a model for obtaining a balance between size and cost, where size is a function of efficiency.

2) SUPPRESSED FE LOSS TECHNOLOGY

The research directions for reducing the core loss of IMs mainly include control and design. Whether to reduce Fe loss by a design method or control strategy depends on an accurate Fe loss calculation. Since the Fe loss is mainly affected by the magnetic field, accurate calculation of the Fe loss requires the distribution of the motor magnetic field. However, the composition of the motor magnetic field which includes the main magnetic field, harmonic magnetic field, and leakage magnetic field, is very complicated. Therefore, an accurate Fe loss model and simulation tools are needed to analyze the Fe loss of the motor.

Finite element analysis (FEA) is the mainstream simulation tool. Two-dimensional 2D-FEA is the most popular method for analyzing Fe loss since it can achieve relatively high computation accuracy and is convenient to use [61], [62]. However, the 2D-FEA generally does not consider the effect of the motor end shield on the Fe loss. If the influence of the end shield is also taken into account, the computation accuracy of the loss can be further improved. However, this makes the complexity of the equation so much that it needs to be calculated with 3D-FEA [63]. The disadvantages of 3D-FEA are a long simulation time and high computing power requirements. Therefore, some researchers have combined the 2D-FEA and 3D-FEA, that is, the effects of the end shield are calculated by 3D-FEA whereas the other parts are calculated by the 2D-FEA [64]. Moreover, some researchers have proposed an improved 2D-FEA, which has the advantages of 3D-FEA [65].

An accurate Fe loss model is the main basis for designing a fast and accurate controller. Divided by type of equivalent circuit, the Fe loss model can be classified into a parallel model and a series model [66]. The series model connects equivalent resistors and magnetizing inductance in series [67]. In this model, the magnetizing inductance is assumed to be independent of frequency, which means that the series model has a simpler structure and is more convenient. However, this independence leads to a certain degree of distortion of the magnetizing inductance when the frequency changes. The parallel model is the mainstream equivalent model, which equates Fe loss to a set of parallel equivalent resistors and magnetizing inductance [68]–[70]. In [68], a control method for reducing Fe loss is proposed in the d-q coordinate system (d-q). However, this model does not consider the influence of stator leakage inductance, which causes a lower model accuracy. In [69], an improved model that takes into account the influence of stator leakage inductance is proposed. Moreover, some models are equivalent based on the stationary coordinate system [71], [72]. Compared with the model in the d-q, this type of model is more streamlined, however, it is difficult to directly apply vector control because the controlled quantity of the vector control is given from the d-q. Given the limitations of the previous model, some researchers combined other control techniques to study the Fe loss reduction model in a stationary coordinate system [73]–[75]. In [75], combined with direct torque control technology (DTC), a model of Fe loss reduction based on a stationary coordinate system was proposed. This model eliminates the complicated calculations required for d-q transformation but inherits the disadvantages of DTC high torque ripple. In [74], the Fe loss reduction method combined with the high-order sliding mode control technique is proposed without the disadvantage of torque ripple. However, the difficulty of proving the stability of the high-order sliding mode technique has produced very complicated controller designs.

In addition to the model-based method, there are also search methods for controlling Fe loss minimization, that is, the flux level is iteratively changed by measuring the input power until the minimum value of the input power is detected [76], [77]. Compared with the model-based method, the search method is not affected by the motor parameters, but the calculation speed is slow. Furthermore, some scholars have proposed hybrid loss minimization control techniques that take advantage of model-based (fast) and search (high accuracy) [78], [79]. This method calculates the approximate optimal magnetic flux that correspond to the minimum loss based on the model and then uses the search algorithm to approximate the optimal magnetic flux.

3) EFFICIENCY IMPROVEMENT STRUCTURE DESIGN

Regarding the structural design of loss suppression, increasing the motor shaft length is a simple method [80]. This method only needs to increase the material of the motor and does not need to re-manufacture the mold, but it may reduce the torque density without redesign. Considering the torque performance, some scholars have proposed a skew rotor loss suppression structure [81]–[83]. This structure can simultaneously improve efficiency and torque. In addition, for the design of manual tuning, it is difficult to ensure that the design is optimal and minimize other performance sacrifices. Some scholars have proposed a multi-objective parameter optimization method [84]–[86], which renders the motor design faster and more balanced in performance.

4) SUMMARY OF IM EFFICIENCY IMPROVEMENT METHODS

We summarize methods for improving the IM efficiency in Table 4. Via topology techniques and parameter optimization design, the efficiency and torque density of the IM are the same as those of the PMSM (Toyota Prius 2010). Combined with mature techniques, the IM has become a low-cost motor solution for high-performance EVs. However, with the development of PM motor techniques and increasingly important endurance requirements in the future, IM's competitiveness in the high-performance EV market will decrease.

V. THE MAIN DEFECTS OF SRM AND THE CURRENT COMPENSATION METHOD

SRM has some shortcomings that hinder its application in EVs. However, the cost of the SRM is lower than the cost of other motors. For the condition of the same output power of 30 kW, the material cost of SRM is approximately half of the material cost of the PMSM (NdFeB) and less than 80% of the material cost of the IM. If shortcomings of the SRM can be compensated, the SRM may be able to provide low-cost solutions for EV propulsion systems. In this chapter, we summarize and compare compensation methods to mitigate the shortcomings of the SRM.

A. INCREASE SRM TORQUE DENSITY

1) HIGH SATURATION FLUX DENSITY MATERIAL

To improve the torque density, we need to improve the magnetic and electric loading for a machine [87]. High saturation flux density material can effectively improve the magnetic loading of a machine. For example, Co-Fe type material has a high saturation flux density that can satisfy this condition, but it is so prohibitive that its application in an EV is not practical. To reduce the cost of EVs, silicone steel was proposed for the replacement of Co-Fe type material in a SRM [88]. Nevertheless, the core loss of silicone steel is much higher than that of Co-Fe-type material, which sacrifices the efficiency of the SRM.

2) MOTOR TOPOLOGY DEVELOPMENTS

Some structures were designed to increase the torque density of SRMs. In [89], a new structure of the SRM, namely, the axial-flux SRM was introduced, which enables efficient utilization of the inner bore and coil end space. To further increase the torque density, the relationship between torque density and axial length (stator pole length, rotor pole length, and rotor yoke thickness) was investigated [90], [91]. According to this relationship, three parameters (stator pole length, rotor pole length, and rotor yoke thickness) of axial length were separately optimized, and a maximum torque density of 47 Nm/L was obtained, which considers the three parameters [90], [91]. The optimization of the stator sectional area could improve the torque density to 51 Nm/L regardless of the heat dissipation.

Other strategies focused on the optimization of shapes and numbers of the stator/rotor pole to improve the torque densities of EV motors. In [92], a design scheme that considered the relationship between the stator/rotor pole arc (βs, βr) and the torque density was proposed to enhance the torque density to 30 Nm/L. However, the torque density of the SRM, which was optimized by changing the stator/rotor pole arc, is limited and is not comparable to that of the PM motor. In [93], engineers designed a new SRM with a torque density of 45 Nm/L, which rivaled the PM motor of that era. This design increased the number of stator poles and expanded the stator taper angle. The increased number of stator poles caused an increase in the stack length of the stator and a decrease in the coil end lengths, which elevates the magnetic loading capacity. Moreover, expanding the stator taper angle is equivalent to increasing the slot fill, which can increase the electric loading capacity. However, this design is only suitable for medium- and high-speed ranges. By changing the shape parameters of the stator/rotor, researchers acquired the same torque density (45 Nm/L) in all speed ranges [94]. These methods only pursue high torque density without considering the influence of other indicators that are also important for the EV, such as torque ripple, noise, and vibration. Apart from perfecting the mechanical parameter and construction of an EV motor, multi-objective optimization, including torque density, was

TABLE 4. Summary of methods for the improvement of IM efficiency.

Method	Adopted technology	Advantage	Reference
Copper loss suppression method			
Increase conductivity	Use copper conductors instead of aluminum conductors	Increase conductivity, Reduce copper loss	[53, 55]
Iron loss suppression technology			
Improve model calculation accuracy	3D finite element analysis	Improve calculation accuracy	[65-67]
Control technology based on Fe loss model	Combination of Fe loss model and vector control	Separately control the two components of speed and magnetic field, Reduce Fe loss	[70-72]
	Establish a controller based on the stationary coordinate system	Simplified model, less calculation, Reduce Fe loss	[73, 74]
	Combination of Fe loss model and DTC	Torque response is faster, Reduce Fe loss	[75, 77]
	Combination of Fe loss model and sliding mode control	Improve robustness, Reduce Fe loss	[76]
Search method	Iterative flux to reduce input power	Not sensitive to motor parameters, Reduce Fe loss	[78, 79]
Combine search and model	First use the Fe loss model to calculate the approximate value of the magnetic flux and then search for the optimal value	Relatively high accuracy, faster calculation speed, Reduce Fe loss	[80, 81]
Efficiency improvement structure design			
Method	Efficiency (%)	Torque Density (Nm/L)	Advantage	Reference
Increase axial length	88 (estimated)	No mention	Simple to implement, Improve efficiency	[82]
Skew rotor structure	87.3	33.17	Improve efficiency and improve torque performance	[83-85]
	86.4	36.17		
Multi-objective optimization	89	15.4	Take into account other performances to maximize efficiency	[86-88]
	86.5-87.7	22.4-39.1		
PMSM Toyota Prius 2010				
N/A	90	33.4	N/A	[40]

proposed in [95], [96]. In [96], a single objective function with multi-geometry-parameters-variables was defined as a weighted sum of the individual criteria for showing the degree of comprehensive optimization. These geometric parameters imply torque, torque ripple, efficiency, and torque density. The author determined the extreme value of the objective function, which was the trade-off point between multiple performances. The effects of the structural optimization and topology design are summarized in Table 5. Compared with the PMSM (Toyota Prius 2010), the torque density of the SRM has increased to the level of the PMSM (Toyota Prius 2010).

B. REDUCE SRM AUDITORY NOISE

Auditory noise is one of the obstacles that prevents extensive use of the SRM in an EV [97]. Vibration noise is generated by the variation in the rotor poles radial force during the phase commutation. Hence, the essence of reducing noise lies in the reduction of the variation in radial force that underlies the stator/rotor topology alternation and current control strategy.

1) STATOR/ROTOR TOPOLOGY DEVELOPMENTS

Some methods reduce radial vibration by improving the stator/rotor topology. In terms of the stator topology, some researchers proposed installing rigid and nonmagnetic structural stator spacers in slot wedges to reduce vibration [98]. However, this modification reduced the winding space. The other topology, the double stator structure, was proposed in [99], [100], in which the rotor was assembled between the inner stator and the outer stator, and thus, the radial force can be counteracted. However, this structure does not reduce wind space; instead, the manufacturing process is complicated. In terms of rotor topology, a cylindrical rotor design, where the salient poles were connected with thin ribs, was proposed in [101]. It can reduce the acoustic noise at high speed.

A structure that was designed to reduce noise by skewing the stator and rotor poles was developed in [102]. Other

TABLE 5. Summary and comparison of torque density increase techniques.

Torque density (Nm/L)	Method of improving torque density	Advantage of method	Reference
Less than 15	Use higher saturation flux density material	Improve torque density	[111]
51	Increase axial length; change stator shape and winding width	Improve torque density	[92, 93]
30.3	Find the maximum torque density corresponding to the stator/rotor pole arc (β_s,β_r,)	Improve torque density, Decrease workload before manufacturing	[94]
45	Increase the number of stator pole; expand the stator taper angle	Improve torque density, Improve efficiency,	[95]
45	Optimize the shape parameters of stator/rotor	Improve torque density, Expand the speed range of optimal performance coverage	[96]
Between 15 and 45	Find the optimal comprehensive performance corresponding to the stator/rotor pole arc(β_s, β_r,) , and the stator pole taper angle	Improve torque density, Decrease torque ripple	[97]
Between 15 and 45	Use two phase excitation modes; Calculate 6 geometry parameters to meet 4 indicators	Optimize torque, torque ripple, efficiency, and torque density	[98]
	PMSM (Toyota Prius 2010)		
33.4	N/A	N/A	[40]

researchers have further investigated the relationship between skewing angles of stator/rotor pole and noise [103], [104], and concluded that skewing the stator pole can reduce more vibration than skewing the rotor pole.

2) CONTROL STRATEGY IMPROVEMENTS

a: INDEPENDENT CONTROL OF POLE CURRENTS

Traditional current control is a kind of three-phase current control, in which each phase current synchronously excites multiple stator poles. In independent pole current control, the stator poles do not have to be simultaneously excited, and each stator pole can be individually excited [105], [106]. Since the conduction angle of each pole can be controlled individually, the desired radial force can be easily generated and the control accuracy of the torque is also improved. However, separate excitation requires a separate power switch for each pole, which increases the cost of the power converter circuit. Moreover, increasing the number of power switches increases the number of switching losses, which affects the efficiency, especially in the high-frequency operating state of the power switch. For instance, for high rotation speeds, the impact on efficiency will be more serious.

b: HYBRID EXCITATION

In [107], [108], the researchers proposed a hybrid excitation method that combined one-phase activation and two-phase activation. In this method, the next phase was activated before the previous phase reached the turn-off angle, and thus, vibration can be reduced in the overlapped region.

c: RANDOMIZING TURN-on/OFF ANGLE

The randomizing turn-on/off angle method was proposed to reduce the noise caused by resonance [110], [111]. Resonance is generated when the radial force frequency coincides with the natural frequency of the motor. In this method, the turn-on/off angle is randomly advanced or delayed within an appropriate limit to expand the frequency spectrum of the radial force and reduce the possibility of resonance. However, the determination of the random range of the turn-on/off angle is a complex problem. If the range is too wide, the overlapping width may be too wide to cause negative torque or too narrow to reduce the torque generating ability [112]. However, if the random range is too small, the radial force spectrum widening effect is not significant. Therefore, it is necessary to conduct in-depth research on the relationship between the random range and the radial force spectrum to determine the optimal random range of the turn-on/off angle to reduce the resonance noise.

d: RADIAL FORCE HARMONICS REDUCTION STRATEGY

The radial force harmonics reduction strategy (RFH) is another noise reduction method for resonance [113], [114]. Different from the idea of widening the radial force harmonics spectrum in the random angle method, the idea of the RFH is to derive a method for eliminating harmonics by analyzing the harmonic model. In [114], the researchers analyzed the relationship between harmonics and the turn-on/off angle based on a simplified harmonic model and then proposed a method for reducing the resonance noise according to this relationship. It can be seen from the simulation results that the

more advanced the turn-on angle is, the smaller the harmonic auxiliary value is. However, the advanced turn-on angle will cause the phase current to increase rapidly before reaching the overlapping position because the inductance is lower at this time. In addition, the lower inductance will produce large phase currents but a smaller torque. Consequently, the large phase current is wasted, which leads to a decrease in efficiency.

e: TWO-STAGE COMMUTATION

A two-stage commutation strategy was proposed in [115]–[118] to solve the vibration caused by the current flow back when both the upper switch and the lower switch were turned off in the nonconduction region. Compared with the traditional switch control scheme, this strategy does not simultaneously turn off the lower switch by turning off the upper switch. Instead, the turn-on time of the lower switch is appropriately prolonged to reduce the backflow current.

3) COMPARISON OF RADIAL VIBRATION MITIGATION TECHNIQUES

Summary the Radial Vibration Mitigation Techniques: Gan *et al.* summarized the radial vibration mitigation techniques () that can reduce the acoustic noise. Based on their summary, we add two methods that can reduce the resonance noise.

C. MITIGATE SRM TORQUE RIPPLE

High torque ripple is one of the factors that hinders the SRM application in EVs. To reduce torque ripple, many advanced techniques that focus on the topology and current control development have been proposed.

1) MOTOR TOPOLOGY DEVELOPMENTS

a: NUMBER OF STATOR/ROTOR POLES

In the past few years, some new designs were presented to produce smooth torque by increasing the number of stator and rotor poles in [120]–[122]. In [120], a novel SRM was developed by increasing the number of rotors. However, this design sacrifices maximum torque performance while reducing torque ripple. Therefore, the optimization needs to consider other indexes. In [121], [122], other parameters, such as the stator/rotor pole arc angle, winding connection, and electromagnetic performance, were investigated to improve the overall performance, including torque ripple.

b: POLE SHAPE DESIGN

In addition to the number of stator/rotor poles, the pole shape was also investigated to reduce torque ripple [123]–[130]. A topology with a notched hole in rotor poles was investigated in [124], [128]. From this design, torque ripple was reduced while maintaining a constant average torque. In [126], another kind of rotor topology, in which a pole shoe is attached to the lateral face of the rotor, was presented to improve the average torque and simultaneously reduce torque ripple. In terms of the stator pole optimization, a special stator pole face shape for reducing torque ripple is proposed in [125]. The author investigated the two different slant directions of the stator: in the first case, the air gap gradually increased during the alignment of the stator pole and rotor pole; in the second case, the air gap was gradually decreased in the quasi-process. It can be seen from the results that regardless of the slanting direction, the higher the stator pole is slanted, the larger the torque ripple is and the larger the average torque is.

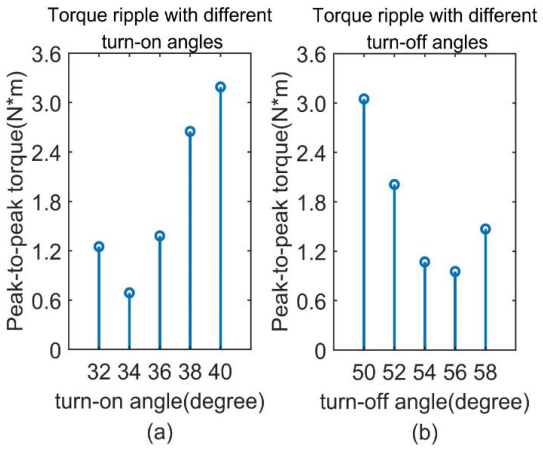

FIGURE 6. (a) Torque ripple at different turn-on angles with the CCC control strategy when the turn-off angle is fixed at 52°; (b) Torque ripple at different turn-off angles with the CCC control strategy when the turn-on angle is fixed at 37°.

2) CONTROL STRATEGY IMPROVEMENTS

a: CURRENT AND ANGLE MODULATIONS

Angle optimization methods [131]–[133] and current profiling methods [134]–[138] are traditional control strategies that can reduce torque ripple. The angle optimization method is to reduce torque ripple by selecting the appropriate switching angle. Generally, the turn-on angle is fixed to adjust the turn-off angle or the turn-off angle is fixed to adjust the turn-on angle. The effect of the different switching angles of the four-phase SRM on torque is shown in FIGURE 6, where (a) is the motor torque at different turn-on angles when the turn-off angle is 52 degrees with current chopping control (CCC) and (b) is the torque at different turn-off angles when the turn-on angle is 37 degrees with CCC. It can be seen from FIGURE 6 (a) that when the turn-off angle remains unchanged, the appropriate decrease in the conduction angle can suppress torque ripple and increase the average torque. However, if the conduction angle decreases too much, torque ripple increases instead, because the inductance slope is too small at this time so that the torque/ampere is low. Nevertheless, as the inductance slope gradually increases, the torque generated by the large current will rapidly increase, which produces a large torque ripple. It can be seen from FIGURE 6 (b) that a fixed turn-on angle increases the turn-off angle to effectively suppress torque ripple. However, the increase in the turn-off angle must be

TABLE 6. Summary and comparison of radial vibration mitigation techniques [119].

Method	Adopted technique	Advantage	Disadvantage	Reference
Inserted stator spacers	Replace the slot wedges with structural stator spacers	Reduce radial vibration, Reduced windage loss, robust structure	Complicated fabrication, difficult installation	[100]
Cylindrical rotor	Connect salient rotor poles with thin ribs	Reduced radial vibration, reduce windage loss, improve efficiency	Thin rib causes deformation at high rotational speed	[103]
Double stator	Assemble the rotor between the inner stator and outer stator	Reduce radial vibration, high power density	High cost for motor prototype, Complicated motor structure	[101, 102]
Skewed poles	Skew the stator and rotor poles with proper angles	Reduce radial vibration, controlled with conventional schemes	Complicated fabrication with different stacks between two laminations	[104-106]
Independent control of poles currents	Each pole winding is independently connected, two additional poles are energized to produce the desired radial force	Radial force and torque can be controlled independently, the desired radial force can be achieved	High cost for more used switching devices, produce negative torque, lower system efficiency	[107, 108]
Hybrid excitation	Combine one-phase excitation and two-phase excitation	Noise and vibration are reduced by hybrid excitation, high efficiency, short tail current, easy to implement	Increased tail current, easily generate negative torque, reduced torque ability	[109, 110]
Two-stage commutation	Add a zero-voltage loop when the corresponding phase is turned off	Reduced radial vibration, easy to implement	Increased tail current, easily generate negative torque, reduced torque ability	[117-120]
Randomizing turn-on/off angle	Randomly determine conduction angle; expand radial force spectrum to avoid natural frequencies	Reduce resonance noise, easy to implement	easily generate negative torque, easily reduced torque ability	[112, 113]
Radial force harmonics reduction strategy	Regulating the turn-on/off angle to eliminate radial force harmonics	Reduce resonance noise	lower system efficiency	[115]

limited to a certain range, because a large turn-off angle will extend the tailing current to the inductance drop zone, which produces negative torque.

The current modulation method controls the torque by tracking the current profiling, which corresponds to the torque from the static current characteristic. To conserve computing power, a lookup table can be used to read the torque value and corresponding current profiling. However, this method requires a substantial amount of memory to store the current profiles so that the resolution can reach the level of identifying small torque changes. Hence, the control effect is very dependent on the accuracy of the static characteristic data.

b: TORQUE SHARING FUNCTION (TSF)

In traditional SRM control, torque ripple is particularly enhanced during commutation because the previous phase does not generate torque when it is deactivated and the next phase does not produce adequate torque during phase commutation [139]. To mitigate torque ripple in commutation, torque sharing function (TSF) control is employed. TSF-based control reduces torque ripple by optimizing the phase reference torque to ensure that the sum of the phase torques in the commutation zone is equal to the average reference torque. The definition of the TSF function depends on the turn-on/off angle and the overlap angle. Common TSF types are linear, exponential, cubic, and sinusoidal. FIGURE 7 shows the typical profiles of the linear TSF, sinusoidal TSF and exponential TSF. FIGURE 8 shows a

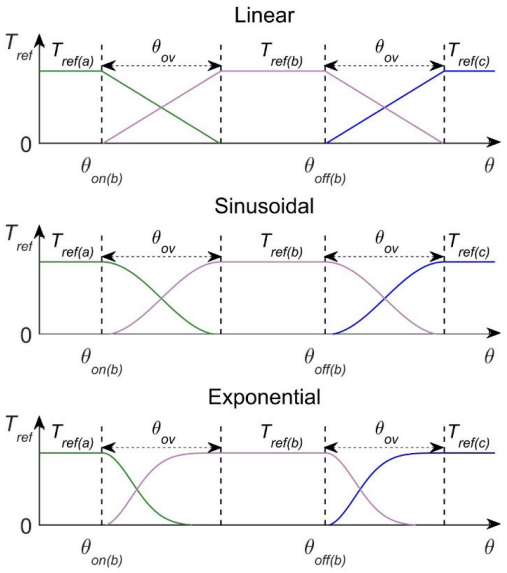

FIGURE 7. Typical profiles of the linear TSF, sinusoidal TSF and exponential TSF.

block diagram of the TSF-based torque control scheme of the conventional three-phases SRM [140]. Each phase reference torque (T_{a_ref}, T_{b_ref}, T_{c_ref} T_{a_ref}, T_{b_ref}, T_{c_ref}) is allocated by the TSF according to the average reference torque ($T_{e\_ref}T_e$) and rotor position ($\theta\theta$). Each phase reference current (i_{a_ref}, i_{b_ref}, i_{c_ref} i_{a_ref}, i_{b_ref}, i_{c_ref}) is obtained by searching the current-position-torque characteristic table to produce a control signal and maintain a total torque constant.

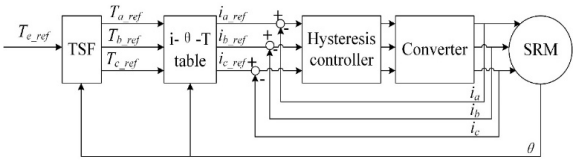

FIGURE 8. Block diagram of TSF based torque control scheme [140].

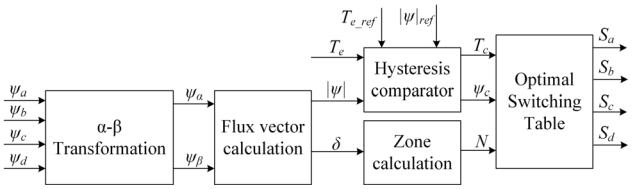

FIGURE 9. Block diagram of DTC controller.

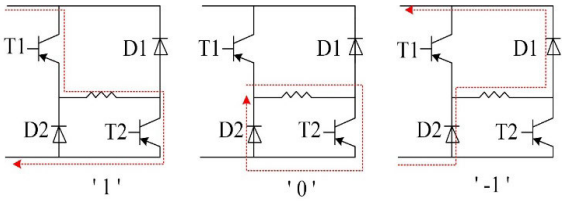

FIGURE 10. Single-phase switch state definition.

By using TSF based control, torque ripple during commutation is effectively eliminated. Some improvements have been made on the TSF to achieve better performance and lower torque ripple [141]–[144]. In [141], to maximize the speed range and to reduce the copper loss, the TSF was improved by using a genetic algorithm to optimize the turn-on/off angle, overlap angle, and expected torque. In [142], an optimized TSF which enabled a balance between copper losses and maximize speed was introduced. However, the TSF only works when the actual current rate of change is greater than that of the reference. Moreover, the actual current rate of change is inversely related to the speed, which causes the reference determined by the TSF to be untracked and poor torque-speed performance at high speeds. To solve this problem, in [143], the defined region of the TSF was extended to the negative torque region to have enough time to raise or decrease the current in the positive torque region. Another scheme for improving tracking was proposed in [144] in which the researcher added a compensator for the torque error generated by the imperfect phase current track.

c: DIRECT TORQUE CONTROL (DTC)

Direct Torque Control (DTC) is a control strategy that considers torque as the direct control object for the alternating current (AC) speed regulation system. DTC selects an appropriate voltage vector based on the deviation between the reference amplitude and the actual value of the torque and flux linkage and then controls the converter to keep the motor torque and flux linkage near the reference value. Because of its reasonable dynamic response to torque changes, some scholars have introduced DTC control into the SRM to suppress torque ripple [145]. Similar to AC motors, the DTC of SRM also selects the voltage vector that is applied to the motor based on the torque and flux linkage amplitude deviation to achieve the purpose of torque control. FIGURE 9 is a block diagram of the DTC controller of the 4-phase SRM (ψ_a, ψ_b, ψ_c, and ψ_d are the flux linkage of each phase of the motor; ψ_a, and ψ_b are the α-axis coordinate and β-axis coordinate, respectively, of the synthetic flux linkage in the α-β coordinate system; $|\psi|$ is the amplitude of the composite flux linkage; δ is the angle of the composite flux linkage and the a-axis; N represents the zone where the composite flux linkage is located; S_a, S_b, S_c, and S_d are the control signals of each phase switch of the converter). It can be seen that DTC does not require static characteristics to estimate parameters, so it can be adapted to motors with the same pole number. However, traditional DTC sector division and voltage vector selection have obvious defects. They are based on the premise that the excitation current can be excited or eliminated instantly. This defect generates negative torque and is not conducive to a reduction in torque ripple during commutation. In response to this defect, some new voltage vector selection rules were proposed in [146], [147]. In [146], the vector selection rule is further subdivided to reduce torque ripple during commutation. In [147], a dynamic sector division rule that changes with the speed and stator current was proposed to demagnetize or excite in advance. This sector division rule reduced not only torque ripple but also negative torque.

Direct instantaneous torque control (DITC) is proposed based on DTC and average torque control (ATC) [148]. Based on DTC, DITC divides the rotation period into several areas and formulates the switching rules of the converter for each area. Compared with DTC, DITC has no hysteresis comparator, and the switch state is only selected according to the torque comparator. The design of the torque hysteresis controller is the core of DITC, and its role is to select the converter switching state that can reduce the torque error according to the area of the rotor position and size of the torque error. The definition of the switch state is shown in FIGURE 10. When both the upper transistors and lower transistors are on, the switch state is defined as '1'; and when only the lower transistor is on, it is defined as '0'; when both the upper transistors and lower transistors are off, it is defined as '−1' [145].

Some DTCs combined with other control methods have been proposed. In [149], the instantaneous torque was controlled by controlling the corresponding co-energy, which was estimated by the current, voltage, and inductance. In [150], a controller was designed based on the Lyapunov function, which can handle the nonlinear characteristics of SRM and increase the robustness of the system by mitigating torque ripple.

d: VECTOR CONTROL

Vector control is a common control method for AC motors. The characteristic of this method is that it can decouple the

excitation current and torque current, and thus, achieving flexible torque control. Some researchers have introduced vector control to SRM control to apply its characteristics to solve the problem of torque ripple [151], [152]. For example, in [151], a hybrid control strategy that combines vector control and continuous current control was proposed, which provided a solution to the problem of torque ripple under high speeds and a heavy load of the SRM.

Unlike traditional angular position control, vector control avoids the need to recalculate the optimal turn-on/off angle of each state due to the different number of rotor poles of the SRM [151]. Because the vector control of the rotor pole pitch is a constant 360° electrical angle, the electrical angle of the angular position control will vary according to the number of SRM rotor poles.

e: MODEL PREDICTIVE CONTROL

The main feature of model predictive control (MPC) is the use of system mathematical models to predict the future behaviors of variables. Each prediction of MPC aims to select the optimal switching state that minimizes the error between the controlled variable and the reference value among all possible converter switching states. Because MPC is intuitive and easy to use, many scholars use MPC to reduce torque ripple of the SRM [153]–[157].

In [155], Mikail proposed a SRM control method that is based on the predicted phase voltage. This control strategy can adjust the PWM duty cycle to achieve accurate current tracking. However, this method needs to further optimize the reference current to achieve the predetermined torque tracking.

In [156], MPC, which predicts torque to achieve torque ripple reduction was proposed. This method provides 30 voltage vectors for the controller to choose the vector that can improve the tracking accuracy. However, a large number of vectors leads to a long search time, which increases the real-time difficulty. Considering this problem, in [154], a faster torque predictive control was proposed by excluding part of the voltage vector and increasing the predictive step width. However, in torque control, the first-order delay between the flux linkage error and the torque error is often disregarded, which causes a delay in torque tracking. Therefore, some scholars designed a direct torque control strategy with low torque ripple based on the method of predicting the flux linkage [157].

f: SLIDING MODE CONTROL (SMC)

SMC is characterized by strong robustness [158], [159], and its design method is not associated with parameters and interference. Therefore, SMC is employed by many scholars to reduce torque ripple in the SRM [160]–[165]. A speed controller that is based on SMC to reduce torque ripple was proposed in [160]. The controller considered the speed error as input, and output the reference current to control the inverter. Considering that the voltage can be used as a control variable to more directly control the inverter, in [162], a sliding mode flux controller with the reference voltage as the output and combined with integral control was proposed to reduce chatting. This method is sensitive to resistance changes, and a small electromotive force at low speeds will cause reduced accuracy. For this reason, Ye *et al.* designed a current controller that is based on SMC, which further improved the robustness of the system compared with the sliding mode flux controller [165]. In addition, some scholars integrated SMC in DTC [161], [163], [164]. For example, in [161] a DTC speed controller with an anti-disturbance synovial observer for compensating the output reference torque was designed based on SMC. The advantage of this kind of method is that the switch state is directly selected to control the torque, and the static characteristics lookup table is not required to switch the current or flux, which conserves storage space.

g: INTELLIGENT CONTROL

Employing classical control theory to control torque requires knowledge of an accurate model of the SRM and solving complex nonlinear equations. This process is cumbersome, and compensation techniques may be needed to reduce system errors. Therefore, the intelligent control method, which achieves a satisfactory control effect without knowledge of an accurate mathematical model of the system, can be regarded as a better solution. Intelligent control includes the following three methods: fuzzy logic control, iterative learning control, and neural network techniques.

Fuzzy control uses language variables to describe a system, which simplifies the complexity of the controller design. The controller design does not depend on a complete mathematical model, so it is suitable for the control of nonlinear systems. Some scholars applied fuzzy control technology to reduce torque ripple in the SRM [166]–[172]. In [166], a SRM torque ripple reduction control system was established based on an adaptive fuzzy control strategy. FIGURE 11 shows the adaptive fuzzy controller for torque control of the SRM. The adaptive fuzzy controller considered the rotor position and torque error as input and output the phase reference current for tracking. Since the controller design does not depend on the SRM mathematical model, it has strong robustness to the SRM with different parameters. However, the adaptive calculation speed is slow, which yields poor dynamic performance. In addition, the accuracy of fuzzy control depends on the number of inputs. Increasing the number of inputs can improve the accuracy but will expand the search range, which increases the difficulty of real-time calculations. Therefore, the SRM system that relies solely on the fuzzy controller can hardly meet the requirements of high dynamic performance and accuracy. Considering these defects, some fuzzy control strategies combined with other control techniques have been proposed to reduce torque ripple. In [168], the fuzzy controller replaced the hysteresis comparator in the DTC and solved the problem of the control signal distortion of the DTC when changing sectors.

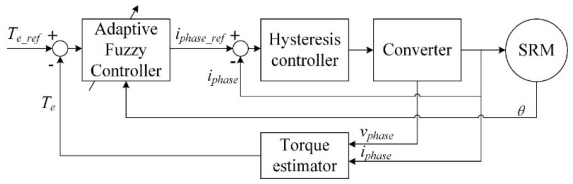

FIGURE 11. Adaptive fuzzy controller for torque control of SRM [167].

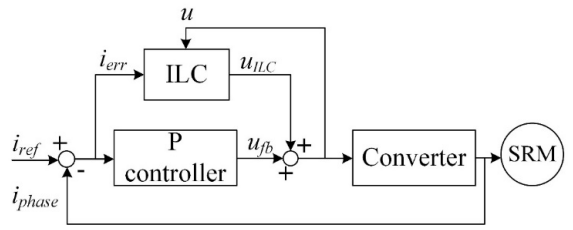

FIGURE 12. Block diagram for ILC-based current controller [173].

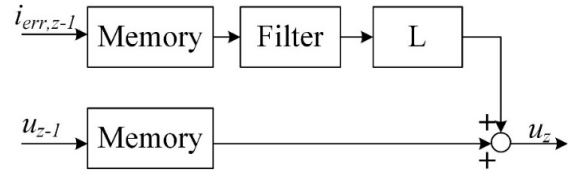

FIGURE 13. Details of ILC block in the current controller [173].

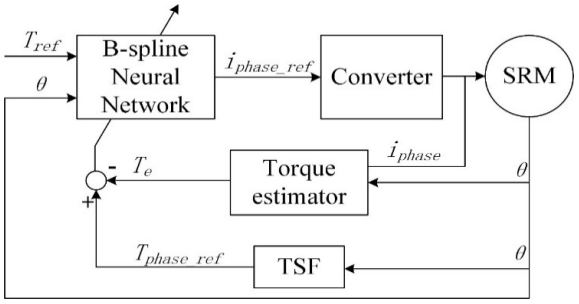

FIGURE 14. Diagram of B-spline neural network scheme [177].

Moreover, this design took advantage of the satisfactory dynamic performance of the DTC.

Some scholars have proposed to design a fuzzy controller to compensate for the control signal, which reduces torque ripple caused by the nonlinearity of the SRM model [167], [169]–[172].For example, in [170], the fuzzy controller was employed to compensate for the current tracking error caused by the tail current and excitation delay in the TSF control at high speeds. In [171], a signal compensation strategy that is based on the neuro-fuzzy method was proposed. The added neural network system can learn according to the compensation signal output by the fuzzy controller to adapt to different operating points.

Iterative learning control (ILC) improves the tracking performance by learning the required control input from a repetitive operation. The mechanism of learning is to store the control input and system output error of each iteration. To minimize the error, the control inputs are adjusted according to a learning law until the error is less than the specified value. FIGURE 12 and FIGURE 13 show details of the ILC block in the SRM controller and the block diagram for the ILC-based current controller, respectively [173]. From the controller, we discover that the system parameters of the SRM do not have to be identified during operation [173]. However, during dynamic conditions, for example, the reference torque is changing, the control effect of the ILC may not be remarkable because the previous memory is not suitable for the tracking present reference. To solve this problem, the P-controller is added to the loop. In addition to be applied in the current controller, ILC is also used to compensate for the output error in the torque-to-current-converter during magnetic saturation [174]. In this way, the converter can provide a more accurate current signal to the controller, and thus, increase the torque tracking speed.

Some scholars utilized a neural network to minimize torque ripple of the SRM [175]–[177] because controller based on neural network did not need knowledge of the motor model and can adjust the control system parameters by self-learning. In [177], a B-spline neural network scheme is employed in torque ripple reduction. By online training with the B-spline neural network, the control system learns the relationship between the two inputs of torque demand and rotor position and the appropriate current profiles to reduce torque ripple. Because the torque demand is introduced to train, this scheme can produce acceptable dynamic performance. FIGURE 14 shows a diagram of the B-spline neural network scheme.

TABLE 7. 8/6 SRM model parameters and control parameters.

8/6 SRM model parameters	
Phase winding resistance (ohm)	1.3
Inertia (kg*m^2)	0.0013
Friction (Nm*s)	0.0183
Maximum inductance (H)	0.092
Minimum inductance (H)	0.022
Maximum current (A)	18
Maximum flux linkage (WB)	0.94
Turn-on (degree)	35
Turn-off (degree)	50

TABLE 8. Peak-to-peak torque of each control.

CCC	TSF	TSF-based DITC	DTC
0.534 Nm	0.365 Nm	0.263 Nm	0.41 Nm

3) COMPARISON OF TORQUE RIPPLE REDUCTION TECHNIQUES

a: SUMMARY OF THE TORQUE RIPPLE REDUCTION TECHNIQUES

Gan *et al.* summarized the torque ripple reduction techniques (Table 9) [119]. Based on their summary, we add one method that corresponds to these techniques.

b: SIMULATION AND COMPARISON

We simulate TSF-based control, DTC, and TSF-based DITC using MATLAB/SIMULINK and apply current chopper

TABLE 9. Summary and comparison of torque ripple reduction techniques [119].

Method	Adopted technique	Advantage	Disadvantage	Reference
High number of rotor poles	Design the rotor with more pole number	Increased average torque, reduce torque ripple in no-saturation condition, reduced copper loss	Complicated rotor configuration, increased rotor materials	[122-124]
Pole shape design	Modification for desired rotor shapes, including pole arc, pole shoe and nonuniform air gap	Lower torque ripple, increased efficiency, high-speed operation performance	Complicated optimization for offline calculation	[125-132]
Current and angle modulation	Optimize the turn-on and turn-off angles or find required current profiles	Improved efficiency, enhanced torque-speed capability, lower torque ripple, realized easily	Current and torque cannot be flexibly controlled, need a large memory to store current profiles	[133-140]
ATC/DTC	Regulate torque by a hysteresis controller with torque estimation	Direct controlled instantaneous torque, reduced torque ripple at a desired level	Need priori-knowledge of machine parameters	[148-152, 159, 180-182]
TSF based method	Definition of TSF profiles, implement hysteresis control with current reference derived for the torque reference	Easily controlled torque, determined torque waveforms, smooth torque over a wide speed range	Need i-T-ϑ characteristics, offline designed torque waveforms	[141, 143-146]
Model predictive control	Predict and control the changes of state variables based on mathematical models	Intuitive, realized easily, Ability to eliminate some theoretical tracking delay, lower torque ripple	High precision requires high sampling rate and strong computing power, which increases the cost of digital controllers	[155-159]
Sliding mode control	Design a controller using sliding mode control theory	Strong robustness, less affected by parameters, strong anti-interference ability	Complicated controller design, high computing power required, Existential chatting	[162-167]
Vector control	Regulate torque under d-q rotating frame	lower torque ripple, No need for angle decoder	Complicated d-q transform	[153, 154]
Intelligent control	Use neural network and other algorithms to design controllers or compensators that do not rely on SRM mathematical models	strong self-learning, adaptive ability, reduced torque ripple, no rely on machine parameters	Complex computational algorithm, real-time difficult	[168-179, 183, 184]

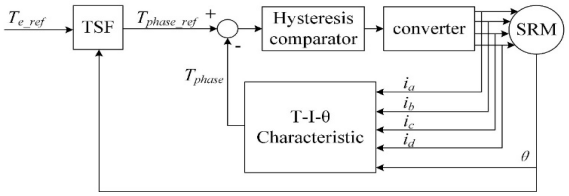

FIGURE 15. Block diagram of TSF-based DITC.

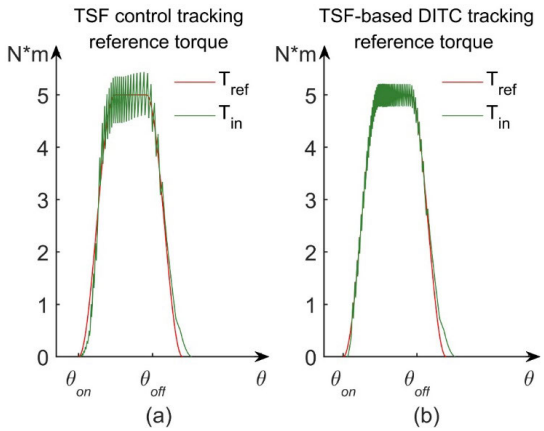

FIGURE 16. TSF and TSF-based DITC tracking effect on reference torque (a) is TSF control strategy, (b) is TSF-based DITC control strategy.

control (CCC) as a comparison object to study the effect of reducing torque ripple. The control block diagram of TSF-based DITC is shown in FIGURE 15. A four-phase 8/6 SRM with a rated power of 8 kW and a rated speed of 300 r/min was selected for simulation. The model parameters and control parameters of the SRM are shown in Table 7. The reference torque is set to 1 Nm.

The torque, flux linkage, and current of the four control strategies, including CCC, TSF, TSF-based DITC, and DTC are compared in FIGURE 17, and the torque ripple of each control strategy is represented by the peak-to-peak torque in Table 8. It can be seen from FIGURE 17 (a, b, c) that in the commutation area, torque ripple increases significantly because, at the beginning of commutation, the next phase fails to quickly generate sufficient torque. To solve this problem, the TSF optimizes the phase torque reference value, that is, the sum of the reference torque of each phase at any time is equal to the average reference torque. The reference current that corresponds to the reference phase torque is calculated according to the static characteristics and subtracted from the actual current to obtain the current error for outputting the control signal to the converter. The torque ripple of the TSF-based torque control shown in FIGURE 17 (b) is 0.3 Nm, which uses a sine function as the torque distribution function. Compared with the torque ripple of 0.8 Nm in FIGURE 17 (a), TSF control has an obvious suppression effect on torque ripple.

In the TSF-based DITC, the instantaneous phase torque directly adjusts the comparison result of the reference torque and the instantaneous torque estimated by the static characteristics according to the torque hysteresis controller. By this strategy, the torque can be adjusted directly based on the

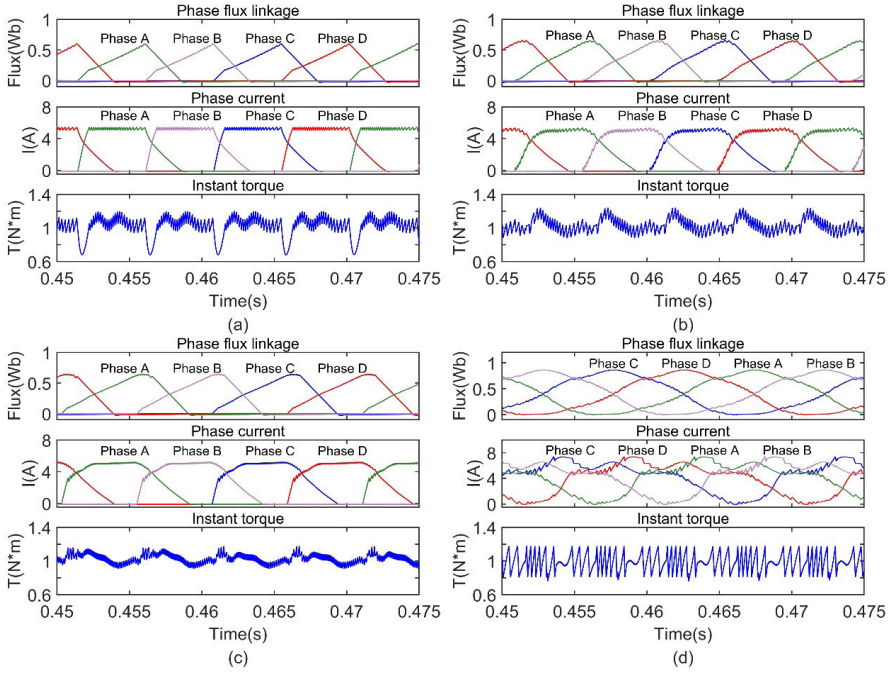

FIGURE 17. Torque, current and flux diagram of 4 control strategies of 8/6 SRM. (a) CCC control strategy, (b) TSF control strategy, (c) TSF-based DITC control strategy, and (d) DTC control strategy.

torque error rather than indirectly adjusted based on the current error. Therefore, the tracking effect of the reference torque is better. FIGURE 16 compares the phase torque tracking effect of the two control strategies (Tref is the reference torque; Tin is the instant torque).

In the DTC control strategy, the flux linkage is maintained at a constant value, and torque control is achieved by adjusting the flux linkage phase angle. In the simulation of DTC, the reference flux linkage is 0.85 Wb, and the torque hysteresis comparator is set to ± 0.2. It can be seen from the torque in FIGURE 17 (d) that DTC does not increase the torque ripple caused by commutation, because DTC does not restrict the switching angle. However, without the constraint of the switching angle, each phase current covers almost the entire rotation cycle, which will produce a large negative torque and reduce the system efficiency.

Compared to the CCC strategy, the three control strategies have effectively suppressed torque ripple. The implementation of TSF-based torque control is relatively simple, and the performance of other aspects can be improved by optimizing the TSF function. For example, it is proposed in [143, 144] to reduce copper loss. Combining DITC and TSF provides better torque ripple suppression but increases the control complexity. DTC has a reasonable control effect on the flux linkage and does not depend on the static characteristics (TSF-based torque control requires i-T-θ characteristics to calculate the reference current, whereas TSC-based DITC requires T-i-θ characteristics to calculate the phase instant torque). However, DTC will produce a large negative torque and reduce the efficiency of the system.

VI. CONCLUSION

To solve the environmental problems caused by transportation, the popularization of EVs is very important and urgent. Currently, short mileage and high cost are the main reasons that hinder the popularization of EVs, and they are closely related to electric motor technology. To solve these two problems, the motor system needs to overcome many challenges in the future. We reviewed the challenges and compensation methods faced by different EV motors to achieve long-range, low-cost EVs. The prospects of each motor application in EV are analyzed.

The rare earth PMSM has high efficiency, high torque, the best mileage performance and the highest cost compared to other motors with the same power. Therefore, this PMSM is suitable for high-performance EVs that are not sensitive to cost. The topology of the PMasyRM and spoke-type motors with rare earth-free PM can effectively reduce the cost of the motor and achieve higher efficiency and torque. Some rare earth-free PM motors that target the rare earth PMSM (Toyota Prius 2010) have been designed. It can be predicted that among the EVs whose torque performance requirements are similar to those of the PMSM (Toyota Prius 2010), rare earth-free PM motors will become increasingly competitive due to their cost advantages.

The IM is currently one of the main options for EVs. The low efficiency rate does not renders this IM conducive to long mileage, which is the main challenge of the IM to overcome. The current topology technology and parameter optimization design can improve the efficiency of the IM to that of the PMSM (Toyota Prius 2010). Therefore, combined with

mature technology, the IM has become a low-cost motor solution for high-performance EVs. However, with the development of PM motor technology and the increasingly important long mileage requirements in the future, the competitiveness of the IM in the high-performance EV market will decrease.

The SRM has obvious advantages in the material cost. Considering its shortcomings of low torque density, high noise, and large torque ripple, the SRM is rarely installed in EVs. In recent years, there have been many excellent results in the research on improving the torque density of SRM, and the same torque performance of the PMSM (Toyota Prius 2010) has been achieved. There are also new developments in the techniques of reducing noise and torque ripple, including control strategies and topology design. These techniques do not affect the material cost of the motor and reduce the research and development costs of EV manufacturers. Therefore, the SRM is expected to become the solution for the EV motor with the lowest cost and a torque density of 35 Nm/L or less due to its low material cost.

In general, with the development of new technologies, PM motors, IM and SRM can reach the level of PMSM (Toyota Prius 2010) in terms of range-related performance, but there is still a big gap with the rare earth PMSM in the past five years. In contrast, SRM shows obvious advantages in cost terms, but it is still difficult to apply to EVs because of severe torque ripple and noise. In the foreseeable future, the competition between the motor types compared in this article that has not yet appeared will continue. There are good reasons to believe that PMSM and IM, which have been so successful in EV applications in the past 10 years, will face strong competition in the next 10 years to maintain their dominant position in passenger car production.

REFERENCES

[1] Y. V. Fan, S. Perry, J. J. Klemeš, and C. T. Lee, "A review on air emissions assessment: Transportation," *J. Cleaner Prod.*, vol. 194, pp. 673–684, Sep. 2018.

[2] P. Hertzke, N. Müller, S. Schenk, and T. Wu. (2018). *The Global Electric-Vehicle Market is Amped Up and on the Rise*. [Online]. Available: https://www.mckinsey.com/industries/automotive-and-assembly/our-insights/the-global-electric-vehicle-market-is-amped-up-and-on-the-rise

[3] IEA, Paris, France. (2020). *Electric Vehicles*. [Online]. Available: https://www.iea.org/reports/electric-vehicles.

[4] G. L. Brase, "What would it take to get you into an electric car? Consumer perceptions and decision making about electric vehicles," *J. Psychol.*, vol. 153, no. 2, pp. 214–236, Feb. 2019.

[5] M. Günther, N. Rauh, and J. F. Krems, "How driving experience and consumption related information influences eco-driving with battery electric vehicles—Results from a field study," *Transp. Res. F, Traffic Psychol. Behav.*, vol. 62, pp. 435–450, Apr. 2019.

[6] Z. Shahan. (2020). *Large Auto Leasing Company: Electric Cars Have Mostly Lower Total Cost in Europe*. [Online]. Available: https://cleantechnica.com/2020/05/08/large-auto-leasing-company-electric-cars-have-mostly-lower-total-cost-in-europe/

[7] G. Berckmans, M. Messagie, J. Smekens, N. Omar, L. Vanhaverbeke, and J. Van Mierlo, "Cost projection of state of the art lithium-ion batteries for electric vehicles up to 2030," *Energies*, vol. 10, no. 9, p. 1314, 2017.

[8] K. L. V. Iyer, C. Lai, S. Mukundan, H. Dhulipati, K. Mukherjee, and N. C. Kar, "Investigation of interior permanent magnet motor with dampers for electric vehicle propulsion and mitigation of saliency effect during integrated charging operation," *IEEE Trans. Veh. Technol.*, vol. 68, no. 2, pp. 1254–1265, Feb. 2019.

[9] G. Pellegrino, A. Vagati, P. Guglielmi, and B. Boazzo, "Performance comparison between surface-mounted and interior PM motor drives for electric vehicle application," *IEEE Trans. Ind. Electron.*, vol. 59, no. 2, pp. 803–811, Feb. 2012.

[10] R. Akune, K. Akatsu, M. Fujihara, and T. Yamamoto, "Study of high torque density interior permanent magnet synchronous motor with flexible orientation $Nd_2Fe_{14}B$ sintered magnet," in *Proc. 22nd Int. Conf. Electr. Mach. (ICEM)*, Sep. 2016, pp. 578–584.

[11] Z. Yang, F. Shang, I. P. Brown, and M. Krishnamurthy, "Comparative study of interior permanent magnet, induction, and switched reluctance motor drives for EV and HEV applications," *IEEE Trans. Transport. Electrific.*, vol. 1, no. 3, pp. 245–254, Oct. 2015.

[12] J. D. Widmer, R. Martin, and M. Kimiabeigi, "Electric vehicle traction motors without rare earth magnets," *Sustain. Mater. Technol.*, vol. 3, pp. 7–13, Apr. 2015.

[13] A. El-Refaie, T. Raminosoa, P. Reddy, S. Galioto, D. Pan, K. Grace, J. Alexander, and K.-K. Huh, "Comparison of traction motors that reduce or eliminate rare-earth materials," *IET Electr. Syst. Transp.*, vol. 7, no. 3, pp. 207–214, Sep. 2017.

[14] X. Zhang, D. Gohlich, and J. Li, "Energy-efficient toque allocation design of traction and regenerative braking for distributed drive electric vehicles," *IEEE Trans. Veh. Technol.*, vol. 67, no. 1, pp. 285–295, Jan. 2018.

[15] J. Guo, J. Wang, and B. Cao, "Regenerative braking strategy for electric vehicles," in *Proc. IEEE Intell. Vehicles Symp.*, Jun. 2009, pp. 864–868.

[16] P. Fajri, S. Lee, V. A. K. Prabhala, and M. Ferdowsi, "Modeling and integration of electric vehicle regenerative and friction braking for motor/dynamometer test bench emulation," *IEEE Trans. Veh. Technol.*, vol. 65, no. 6, pp. 4264–4273, Jun. 2016.

[17] S. Heydari, P. Fajri, N. Lotfi, and B. Falahati, "Influencing factors in low speed regenerative braking performance of electric vehicles," in *Proc. IEEE Transp. Electrific. Conf. Expo (ITEC)*, Jun. 2018, pp. 494–499.

[18] K. Kiyota, H. Sugimoto, and A. Chiba, "Comparison of energy consumption of SRM and IPMSM in automotive driving schedules," in *Proc. IEEE Energy Convers. Congr. Expo. (ECCE)*, Sep. 2012, pp. 853–860.

[19] Z. Q. Zhu, W. Q. Chu, and Y. Guan, "Quantitative comparison of electromagnetic performance of electrical machines for HEVs/EVs," *CES Trans. Electr. Mach. Syst.*, vol. 1, no. 1, pp. 37–47, Mar. 2017.

[20] G. Pellegrino, A. Vagati, B. Boazzo, and P. Guglielmi, "Comparison of induction and PM synchronous motor drives for EV application including design examples," *IEEE Trans. Ind. Appl.*, vol. 48, no. 6, pp. 2322–2332, Nov. 2012.

[21] M. Zeraoulia, M. E. H. Benbouzid, and D. Diallo, "Electric motor drive selection issues for HEV propulsion systems: A comparative study," *IEEE Trans. Veh. Technol.*, vol. 55, no. 6, pp. 1756–1764, Nov. 2006.

[22] J.-R. Riba, C. López-Torres, L. Romeral, and A. Garcia, "Rare-earth-free propulsion motors for electric vehicles: A technology review," *Renew. Sustain. Energy Rev.*, vol. 57, pp. 367–379, May 2016.

[23] K. Sakai, K. Yuki, Y. Hashiba, N. Takahashi, and K. Yasui, "Principle of the variable-magnetic-force memory motor," in *Proc. Int. Conf. Electr. Mach. Syst.*, Nov. 2009, pp. 1–6.

[24] V. Ostovic, "Memory motors," *IEEE Ind. Appl. Mag.*, vol. 9, no. 1, pp. 52–61, Jan. 2003.

[25] C. Yu and K. T. Chau, "Design, analysis, and control of DC-excited memory motors," *IEEE Trans. Energy Convers.*, vol. 26, no. 2, pp. 479–489, Jun. 2011.

[26] S. S. Maroufian and P. Pillay, "Design and analysis of a novel PM-assisted synchronous reluctance machine topology with AlNiCo magnets," *IEEE Trans. Ind. Appl.*, vol. 55, no. 5, pp. 4733–4742, Sep. 2019.

[27] X. Zhu, L. Quan, D. Chen, M. Cheng, W. Hua, and X. Sun, "Electromagnetic performance analysis of a new stator-permanent-magnet doubly salient flux memory motor using a piecewise-linear hysteresis model," *IEEE Trans. Magn.*, vol. 47, no. 5, pp. 1106–1109, May 2011.

[28] P. B. Reddy, K. Grace, and A. El-Refaie, "Conceptual design of sleeve rotor synchronous reluctance motor for traction applications," in *Proc. IEEE Int. Electr. Mach. Drives Conf. (IEMDC)*, May 2015, pp. 195–201.

[29] T. Miura, S. Chino, M. Takemoto, S. Ogasawara, A. Chiba, and N. Hoshi, "A ferrite permanent magnet axial gap motor with segmented rotor structure for the next generation hybrid vehicle," in *Proc. 19th Int. Conf. Electr. Mach. (ICEM)*, Sep. 2010, pp. 1–6.

[30] K. M. Rahman, N. R. Patel, T. G. Ward, J. M. Nagashima, F. Caricchi, and F. Crescimbini, "Application of direct-drive wheel motor for fuel cell electric and hybrid electric vehicle propulsion system," *IEEE Trans. Ind. Appl.*, vol. 42, no. 5, pp. 1185–1192, Sep. 2006.

[31] W. Zhao, T. A. Lipo, and B.-I. Kwon, "Comparative study on novel dual stator radial flux and axial flux permanent magnet motors with ferrite magnets for traction application," *IEEE Trans. Magn.*, vol. 50, no. 11, pp. 1–4, Nov. 2014.

[32] M. De Gennaro, J. Jürgens, A. Zanon, J. Gragger, E. Schlemmer, A. Fricassè, L. Marengo, B. Ponick, E. T. Olabarri, J. Kinder, A. Cavallini, P. Mancinelli, M. Hernandez, and M. Messagie, "Designing, prototyping and testing of a ferrite permanent magnet assisted synchronous reluctance machine for hybrid and electric vehicles applications," *Sustain. Energy Technol. Assessments*, vol. 31, pp. 86–101, Feb. 2019.

[33] S. Morimoto, S. Ooi, Y. Inoue, and M. Sanada, "Experimental evaluation of a rare-earth-free PMASynRM with ferrite magnets for automotive applications," *IEEE Trans. Ind. Electron.*, vol. 61, no. 10, pp. 5749–5756, Oct. 2014.

[34] M. Kimiabeigi, J. D. Widmer, R. Long, Y. Gao, J. Goss, R. Martin, T. Lisle, J. M. S. Vizan, A. Michaelides, and B. Mecrow, "High-performance low-cost electric motor for electric vehicles using ferrite magnets," *IEEE Trans. Ind. Electron.*, vol. 63, no. 1, pp. 113–122, Jan. 2016.

[35] S. Ooi, S. Morimoto, M. Sanada, and Y. Inoue, "Performance evaluation of a high-power-density PMASynRM with ferrite magnets," *IEEE Trans. Ind. Appl.*, vol. 49, no. 3, pp. 1308–1315, May 2013.

[36] M. Sanada, Y. Inoue, and S. Morimoto, "Rotor structure for reducing demagnetization of magnet in a PMASynRM with ferrite permanent magnet and its characteristics," in *Proc. IEEE Energy Convers. Congr. Exposit.*, Sep. 2011, pp. 4189–4194.

[37] M. Hofer and M. Schrodl, "Investigation of permanent magnet assisted synchronous reluctance machines for traction drives in high power flux weakening operation," in *Proc. IEEE Transp. Electrific. Conf. Expo (ITEC)*, Jun. 2020, pp. 335–339.

[38] K.-C. Kim, J. S. Ahn, S. H. Won, J.-P. Hong, and J. Lee, "A study on the optimal design of SynRM for the high torque and power factor," *IEEE Trans. Magn.*, vol. 43, no. 6, pp. 2543–2545, Jun. 2007.

[39] T. A. Burress *et al.*, "Evaluation of the 2010 Toyota Prius hybrid synergy drive system," Power Electron. Electr. Mach. Res. Facility, Oak Ridge Nat. Lab.(ORNL), Oak Ridge, TN, USA, Tech. Rep. ORNL/TM-2010/253, 2011.

[40] A. Fatemi, D. M. Ionel, M. Popescu, Y. C. Chong, and N. A. O. Demerdash, "Design optimization of a high torque density spoke-type PM motor for a formula e race drive cycle," *IEEE Trans. Ind. Appl.*, vol. 54, no. 5, pp. 4343–4354, Sep. 2018.

[41] W. Kakihara, M. Takemoto, and S. Ogasawara, "Rotor structure in 50 kW spoke-type interior permanent magnet synchronous motor with ferrite permanent magnets for automotive applications," in *Proc. IEEE Energy Convers. Congr. Expo.*, Sep. 2013, pp. 606–613.

[42] M. Onsal, B. Cumhur, Y. Demir, E. Yolacan, and M. Aydin, "Rotor design optimization of a new flux-assisted consequent pole spoke-type permanent magnet torque motor for low-speed applications," *IEEE Trans. Magn.*, vol. 54, no. 11, pp. 1–5, Nov. 2018.

[43] M. Kimiabeigi, R. Long, J. D. Widmer, and Y. Gao, "Comparative assessment of single piece and fir-tree-based spoke type rotor designs for low-cost electric vehicle application," *IEEE Trans. Energy Convers.*, vol. 32, no. 2, pp. 486–494, Jun. 2017.

[44] Y. Chen and B. Zhang, "Minimization of the electromagnetic torque ripple caused by the coils inter-turn short circuit fault in dual-redundancy permanent magnet synchronous motors," *Energies*, vol. 10, no. 11, p. 1798, Nov. 2017.

[45] K. Pietrusewicz, P. Waszczuk, and M. Kubicki, "MFC/IMC control algorithm for reduction of load torque disturbance in PMSM servo drive systems," *Appl. Sci.*, vol. 9, no. 1, p. 86, Dec. 2018.

[46] Y.-F. Jia, L. Chu, N. Xu, Y.-K. Li, D. Zhao, and X. Tang, "Power sharing and voltage vector distribution model of a dual inverter open-end winding motor drive system for electric vehicles," *Appl. Sci.*, vol. 8, no. 2, p. 254, Feb. 2018.

[47] R. Benlamine, F. Dubas, C. Espanet, S. A. Randi, and D. Lhotellier, "Design of an axial-flux interior permanent-magnet synchronous motor for automotive application: Performance comparison with electric motors used in EVs and HEVs," in *Proc. IEEE Vehicle Power Propuls. Conf. (VPPC)*, Oct. 2014, pp. 1–6.

[48] M. Kimiabeigi, B. C. Mecrow, J. D. Widmer, R. Long, Y. Gao, J. Goss, R. Martin, T. Lisle, J. M. S. Vizan, and A. Michaelides, "On selection of rotor support material for a ferrite magnet spoke-type traction motor," *IEEE Trans. Ind. Appl.*, vol. 52, no. 3, pp. 2224–2233, May 2016.

[49] D. R. Crecelius, J. C. Morgante, and J. J. Ronning, "More efficiency with dual motor control in battery electric vehicles," *MTZ Worldwide*, vol. 80, no. 12, pp. 60–63, Nov. 2019.

[50] A. T. De Almeida, F. J. Ferreira, and J. A. Fong, "Standards for efficiency of electric motors," *IEEE Ind. Appl. Mag.*, vol. 17, no. 1, pp. 12–19, Jan. 2010.

[51] S. Mallik, K. Mallik, A. Barman, D. Maiti, S. K. Biswas, N. K. Deb, and S. Basu, "Efficiency and cost optimized design of an induction motor using genetic algorithm," *IEEE Trans. Ind. Electron.*, vol. 64, no. 12, pp. 9854–9863, Dec. 2017.

[52] H. Li and K. W. Klontz, "Rotor design to reduce secondary winding harmonic loss for induction motor in hybrid electric vehicle application," in *Proc. IEEE Energy Convers. Congr. Expo. (ECCE)*, Sep. 2016, pp. 1–6.

[53] D. Gerada, A. Mebarki, N. L. Brown, K. J. Bradley, and C. Gerada, "Design aspects of high-speed high-power-density laminated-rotor induction machines," *IEEE Trans. Ind. Electron.*, vol. 58, no. 9, pp. 4039–4047, Sep. 2011.

[54] J. L. Kirtley, J. G. Cowie, E. F. Brush, D. T. Peters, and R. Kimmich, "Improving induction motor efficiency with die-cast copper rotor cages," in *Proc. IEEE Power Eng. Soc. Gen. Meeting*, Jun. 2007, pp. 1–6.

[55] R. Tiwari and A. Bhardwaj, "Analysis of Induction Motor with die cast rotor," *Int. J. Innov. Res. Electr., Electron., Instrum. Control Eng.*, vol. 2, no. 6, pp. 1–7, Feb. 2014.

[56] G. C. Mechler, "Manufacturing and cost analysis for aluminum and copper die cast induction motors for GM's powertrain and R&D divisions," Dept. Mater. Sci. Eng., Massachusetts Inst. Technol., Cambridge, MA, USA, Tech. Rep., 2010.

[57] S. T. Varghese, K. R. Rajagopal, and B. Singh, "Design and development of rotor quality test system for die-cast copper rotors," *IEEE Trans. Ind. Appl.*, vol. 54, no. 3, pp. 2105–2114, May 2018.

[58] S. Manoharan, N. Devarajan, S. M. Deivasahayam, and G. Ranganathan, "Review on efficiency improvement in squirrel cage induction motor by using DCR technology," *J. Electr. Eng.*, vol. 60, no. 4, pp. 227–236, Aug. 2009.

[59] S. Yamamoto, "Overview of the latest research and development for copper die-cast squirrel-cage rotors," in *Proc. Int. Power Electron. Conf. (IPEC-Niigata -ECCE Asia)*, May 2018, pp. 1949–1954.

[60] Y. Wang, J. Lu, C. Liu, G. Lei, Y. Guo, and J. Zhu, "Development of a high-performance axial flux PM machine with SMC cores for electric vehicle application," *IEEE Trans. Magn.*, vol. 55, no. 7, pp. 1–4, Jul. 2019.

[61] J.-J. Lee, Y.-K. Kim, H. Nam, K.-H. Ha, J.-P. Hong, and D.-H. Hwang, "Loss distribution of three-phase induction motor fed by pulsewidth-modulated inverter," *IEEE Trans. Magn.*, vol. 40, no. 2, pp. 762–765, Mar. 2004.

[62] N. Stranges and R. D. Findlay, "Methods for predicting rotational iron losses in three phase induction motor stators," *IEEE Trans. Magn.*, vol. 36, no. 5, pp. 3112–3114, Sep. 2000.

[63] R. Lin, A. Haavisto, and A. Arkkio, "Analysis of eddy-current loss in end shield and frame of a large induction machine," *IEEE Trans. Magn.*, vol. 46, no. 3, pp. 942–948, Mar. 2010.

[64] K. Yamazaki, "Induction motor analysis considering both harmonics and end effects using combination of 2D and 3D finite element method," *IEEE Trans. Energy Convers.*, vol. 14, no. 3, pp. 698–703, Sep. 1999.

[65] S. Niu, S. L. Ho, W. N. Fu, and J. Zhu, "Eddy current reduction in high-speed machines and eddy current loss analysis with multislice time-stepping finite-element method," *IEEE Trans. Magn.*, vol. 48, no. 2, pp. 1007–1010, Feb. 2012.

[66] K. Wang, R. Huai, Z. Yu, X. Zhang, F. Li, and L. Zhang, "Comparison study of induction motor models considering iron loss for electric drives," *Energies*, vol. 12, no. 3, p. 503, Feb. 2019.

[67] J. Jung and K. Nam, "A vector control scheme for EV induction motors with a series iron loss model," *IEEE Trans. Ind. Electron.*, vol. 45, no. 4, pp. 617–624, Aug. 1998.

[68] G. O. Garcia, J. C. M. Luis, R. M. Stephan, and E. H. Watanabe, "An efficient controller for an adjustable speed induction motor drive," *IEEE Trans. Ind. Electron.*, vol. 41, no. 5, pp. 533–539, Oct. 1994.

[69] M. N. Uddin and S. W. Nam, "Development of a nonlinear and model-based online loss minimization control of an IM drive," *IEEE Trans. Energy Convers.*, vol. 23, no. 4, pp. 1015–1024, Dec. 2008.

[70] C. Chakraborty and Y. Hori, "Fast efficiency optimization techniques for the indirect vector-controlled induction motor drives," *IEEE Trans. Ind. Appl.*, vol. 39, no. 4, pp. 1070–1076, Jul. 2003.

[71] Z. Qu, M. Ranta, M. Hinkkanen, and J. Luomi, "Loss-minimizing flux level control of induction motor drives," *IEEE Trans. Ind. Appl.*, vol. 48, no. 3, pp. 952–961, May 2012.
[72] M. C. Di Piazza, M. Luna, and M. Pucci, "Electrical loss minimization technique for wind generators based on a comprehensive dynamic modeling of induction machines," *IEEE Trans. Ind. Appl.*, vol. 53, no. 4, pp. 3696–3706, Jul. 2017.
[73] F. Tazerart, Z. Mokrani, D. Rekioua, and T. Rekioua, "Direct torque control implementation with losses minimization of induction motor for electric vehicle applications with high operating life of the battery," *Int. J. Hydrogen Energy*, vol. 40, no. 39, pp. 13827–13838, Oct. 2015.
[74] J. R. Dominguez, C. Mora-Soto, S. Ortega-Cisneros, J. J. R. Panduro, and A. G. Loukianov, "Copper and core loss minimization for induction motors using high-order sliding-mode control," *IEEE Trans. Ind. Electron.*, vol. 59, no. 7, pp. 2877–2889, Jul. 2012.
[75] M. Hajian, J. Soltani, G. A. Markadeh, and S. Hosseinnia, "Adaptive nonlinear direct torque control of sensorless IM drives with efficiency optimization," *IEEE Trans. Ind. Electron.*, vol. 57, no. 3, pp. 975–985, Mar. 2010.
[76] A. Taheri, A. Rahmati, and S. Kaboli, "Efficiency improvement in DTC of six-phase induction machine by adaptive gradient descent of flux," *IEEE Trans. Power Electron.*, vol. 27, no. 3, pp. 1552–1562, Mar. 2012.
[77] S. Kaboli, M. R. Zolghadri, and E. Vahdati-Khajeh, "A fast flux search controller for DTC-based induction motor drives," *IEEE Trans. Ind. Electron.*, vol. 54, no. 5, pp. 2407–2416, Oct. 2007.
[78] F. Farhani, A. Zaafouri, and A. Chaari, "Real time induction motor efficiency optimization," *J. Franklin Inst.*, vol. 354, no. 8, pp. 3289–3304, May 2017.
[79] T. R. Chelliah, J. G. Yadav, S. P. Srivastava, and P. Agarwal, "Optimal energy control of induction motor by hybridization of loss model controller based on particle swarm optimization and search controller," in *Proc. World Congr. Nature Biologically Inspired Comput. (NaBIC)*, 2009, pp. 1178–1183.
[80] L. Alberti, N. Bianchi, A. Boglietti, and A. Cavagnino, "Core axial lengthening as effective solution to improve the induction motor efficiency classes," *IEEE Trans. Ind. Appl.*, vol. 50, no. 1, pp. 218–225, Jan. 2014.
[81] Y. Kawase, T. Yamaguchi, Z. Tu, N. Toida, N. Minoshima, and K. Hashimoto, "Effects of skew angle of rotor in squirrel-cage induction motor on torque and loss characteristics," *IEEE Trans. Magn.*, vol. 45, no. 3, pp. 1700–1703, Mar. 2009.
[82] M. T. Guneser, A. Dalcali, T. Ozturk, C. Ocak, and M. Cernat, "An induction motor design for urban use electric vehicle," presented at the IEEE Int. Power Electron. Motion Control Conf. (PEMC), Sep. 2016.
[83] Q. Zhang, H. Liu, Z. Zhang, and T. Song, "A cast copper rotor induction motor for small commercial EV traction: Electromagnetic design, analysis, and experimental tests," *CES Trans. Electr. Mach. Syst.*, vol. 2, no. 4, pp. 417–424, Dec. 2018.
[84] G. Lee, S. Min, and J.-P. Hong, "Optimal shape design of rotor slot in squirrel-cage induction motor considering torque characteristics," *IEEE Trans. Magn.*, vol. 49, no. 5, pp. 2197–2200, May 2013.
[85] D. Zhang, C. S. Park, and C. S. Koh, "A new optimal design method of rotor slot of three-phase squirrel cage induction motor for NEMA class D speed-torque characteristic using multi-objective optimization algorithm," *IEEE Trans. Magn.*, vol. 48, no. 2, pp. 879–882, Feb. 2012.
[86] M. J. Akhtar and R. K. Behera, "Optimal design of stator and rotor slot of induction motor for electric vehicle applications," *IET Electr. Syst. Transp.*, vol. 9, no. 1, pp. 35–43, Mar. 2019.
[87] D. Lu and N. C. Kar, "A review of flux-weakening control in permanent magnet synchronous machines," in *Proc. IEEE Vehicle Power Propuls. Conf.*, Sep. 2010, pp. 1–6.
[88] K. M. Rahman and S. E. Schulz, "Design of high-efficiency and high-torque-density switched reluctance motor for vehicle propulsion," *IEEE Trans. Ind. Appl.*, vol. 38, no. 6, pp. 1500–1507, Nov. 2002.
[89] Y. Ono, K. Nakamura, and O. Ichinokura, "Basic examination of configuration of axial-gap SR motor," *J. Magn. Soc. Jpn.*, vol. 35, no. 2, pp. 106–111, 2011.
[90] H. Goto, S. Murakami, and O. Ichinokura, "Design to maximize torque-volume density of axial-flux SRM for in-wheel EV," in *Proc. 41st Annu. Conf. IEEE Ind. Electron. Soc. (IECON)*, Nov. 2015, pp. 5191–5196.
[91] S. Murakami, H. Goto, and O. Ichinokura, "A study about optimum stator pole design of axial-gap switched reluctance motor," in *Proc. Int. Conf. Electr. Mach. (ICEM)*, Sep. 2014, pp. 975–980.
[92] M. Yildirim, M. Polat, E. Oksuztepe, Z. Omac, O. Yakut, H. Eren, M. Kaya, and H. Kurum, "Designing in-wheel switched reluctance motor for electric vehicles," in *Proc. 16th Int. Power Electron. Motion Control Conf. Expo.*, Sep. 2014, pp. 793–798.
[93] A. Chiba, Y. Takano, M. Takeno, T. Imakawa, N. Hoshi, M. Takemoto, and S. Ogasawara, "Torque density and efficiency improvements of a switched reluctance motor without rare-earth material for hybrid vehicles," *IEEE Trans. Ind. Appl.*, vol. 47, no. 3, pp. 1240–1246, May 2011.
[94] M. Takeno, A. Chiba, N. Hoshi, S. Ogasawara, M. Takemoto, and M. A. Rahman, "Test results and torque improvement of the 50-kW switched reluctance motor designed for hybrid electric vehicles," *IEEE Trans. Ind. Appl.*, vol. 48, no. 4, pp. 1327–1334, Jul. 2012.
[95] M. Cosovic, S. Smaka, I. Salihbegovic, and S. Masic, "Design optimization of 8/14 switched reluctance machine for electric vehicle," in *Proc. 20th Int. Conf. Electr. Mach.*, Sep. 2012, pp. 2654–2659.
[96] Y. Zhu, W. Wei, C. Yang, and Y. Zhang, "Multi-objective optimisation design of two-phase excitation switched reluctance motor for electric vehicles," *IET Electr. Power Appl.*, vol. 12, no. 7, pp. 929–937, Aug. 2018.
[97] M. S. Kumar and S. T. Revankar, "Development scheme and key technology of an electric vehicle: An overview," *Renew. Sustain. Energy Rev.*, vol. 70, pp. 1266–1285, Apr. 2017.
[98] P. O. Rasmussen, J. H. Andreasen, and J. M. Pijanowski, "Structural stator spacers—A solution for noise reduction of switched reluctance motors," *IEEE Trans. Ind. Appl.*, vol. 40, no. 2, pp. 574–581, Mar. 2004.
[99] M. Abbasian, M. Moallem, and B. Fahimi, "Double-stator switched reluctance machines (DSSRM): Fundamentals and magnetic force analysis," *IEEE Trans. Energy Convers.*, vol. 25, no. 3, pp. 589–597, Sep. 2010.
[100] A. H. Isfahani and B. Fahimi, "Comparison of mechanical vibration between a double-stator switched reluctance machine and a conventional switched reluctance machine," *IEEE Trans. Magn.*, vol. 50, no. 2, pp. 293–296, Feb. 2014.
[101] K. Kiyota, T. Kakishima, A. Chiba, and M. A. Rahman, "Cylindrical rotor design for acoustic noise and windage loss reduction in switched reluctance motor for HEV applications," *IEEE Trans. Ind. Appl.*, vol. 52, no. 1, pp. 154–162, Jan. 2016.
[102] H.-Y. Yang, Y.-C. Lim, and H.-C. Kim, "Acoustic noise/vibration reduction of a single-phase SRM using skewed stator and rotor," *IEEE Trans. Ind. Electron.*, vol. 60, no. 10, pp. 4292–4300, Oct. 2013.
[103] Y. Zou, K.-W.-E. Cheng, N. C. Cheung, and J. Pan, "Deformation and noise mitigation for the linear switched reluctance motor with skewed teeth structure," *IEEE Trans. Magn.*, vol. 50, no. 11, pp. 1–4, Nov. 2014.
[104] C. Gan, J. Wu, M. Shen, S. Yang, Y. Hu, and W. Cao, "Investigation of skewing effects on the vibration reduction of three-phase switched reluctance motors," *IEEE Trans. Magn.*, vol. 51, no. 9, pp. 1–9, Sep. 2015.
[105] F.-C. Lin and S.-M. Yang, "Instantaneous shaft radial force control with sinusoidal excitations for switched reluctance motors," *IEEE Trans. Energy Convers.*, vol. 22, no. 3, pp. 629–636, Sep. 2007.
[106] F.-C. Lin and S.-M. Yang, "An approach to producing controlled radial force in a switched reluctance motor," *IEEE Trans. Ind. Electron.*, vol. 54, no. 4, pp. 2137–2146, Aug. 2007.
[107] X. Cao, Z. Deng, G. Yang, and X. Wang, "Independent control of average torque and radial force in bearingless switched-reluctance motors with hybrid excitations," *IEEE Trans. Power Electron.*, vol. 24, no. 5, pp. 1376–1385, May 2009.
[108] J.-W. Ahn, S.-J. Park, and D.-H. Lee, "Hybrid excitation of SRM for reduction of vibration and acoustic noise," *IEEE Trans. Ind. Electron.*, vol. 51, no. 2, pp. 374–380, Apr. 2004.
[109] Z. Qionghua, W. Shuanghong, M. Zhiyuan, G. Wei, and Q. Yihui, "Design of a 50 kW switched reluctance machine for HEV propulsion system," in *Proc. IEEE 58th Veh. Technol. Conf. (VTC-Fall)*, Oct. 2003, pp. 3207–3211.
[110] X.-Q. Guo, R. Zhong, D.-S. Ding, M.-S. Zhang, W.-J. Shao, and W.-F. Sun, "Origin of resonance noise and analysis of randomising turn-on angle method in switched reluctance motor," *IET Electr. Power Appl.*, vol. 11, no. 7, pp. 1324–1332, Aug. 2017.
[111] T. Boukhobza, M. Gabsi, and B. Grioni, "Random variation of control angles, reduction of SRM vibrations," in *Proc. IEEE Int. Electr. Mach. Drives Conf. (IEMDC)*, Jun. 2001, pp. 640–643.
[112] J. Y. Chai, Y. W. Lin, and C. M. Liaw, "Comparative study of switching controls in vibration and acoustic noise reductions for switched reluctance motor," *IEE Proc.-Electr. Power Appl.*, vol. 153, no. 3, pp. 348–360, May 2006.

[113] M. Takiguchi, H. Sugimoto, N. Kurihara, and A. Chiba, "Acoustic noise and vibration reduction of SRM by elimination of third harmonic component in sum of radial forces," *IEEE Trans. Energy Convers.*, vol. 30, no. 3, pp. 883–891, Sep. 2015.

[114] X. Guo, R. Zhong, M. Zhang, D. Ding, and W. Sun, "Resonance reduction by optimal switch angle selection in switched reluctance motor," *IEEE Trans. Ind. Electron.*, vol. 67, no. 3, pp. 1867–1877, Mar. 2020.

[115] C. Pollock and C.-Y. Wu, "Acoustic noise cancellation techniques for switched reluctance drives," *IEEE Trans. Ind. Appl.*, vol. 33, no. 2, pp. 477–484, Mar. 1997.

[116] Z. Q. Zhu, X. Liu, and Z. Pan, "Analytical model for predicting maximum reduction levels of vibration and noise in switched reluctance machine by active vibration cancellation," *IEEE Trans. Energy Convers.*, vol. 26, no. 1, pp. 36–45, Mar. 2011.

[117] H. Makino, T. Kosaka, and N. Matsui, "Digital PWM-control-based active vibration cancellation for switched reluctance motors," *IEEE Trans. Ind. Appl.*, vol. 51, no. 6, pp. 4521–4530, Nov. 2015.

[118] A. Rezig, W. Boudendouna, A. Djerdir, and A. N'Diaye, "Investigation of optimal control for vibration and noise reduction in-wheel switched reluctance motor used in electric vehicle," *Math. Comput. Simul.*, vol. 167, pp. 267–280, Jan. 2020.

[119] C. Gan, J. Wu, Q. Sun, W. Kong, H. Li, and Y. Hu, "A review on machine topologies and control techniques for low-noise switched reluctance motors in electric vehicle applications," *IEEE Access*, vol. 6, pp. 31430–31443, 2018.

[120] P. C. Desai, M. Krishnamurthy, N. Schofield, and A. Emadi, "Novel switched reluctance machine configuration with higher number of rotor poles than stator poles: Concept to implementation," *IEEE Trans. Ind. Electron.*, vol. 57, no. 2, pp. 649–659, Feb. 2010.

[121] B. Bilgin, A. Emadi, and M. Krishnamurthy, "Design considerations for switched reluctance machines with a higher number of rotor poles," *IEEE Trans. Ind. Electron.*, vol. 59, no. 10, pp. 3745–3756, Oct. 2012.

[122] X. Liu and Z. Q. Zhu, "Stator/rotor pole combinations and winding configurations of variable flux reluctance machines," *IEEE Trans. Ind. Appl.*, vol. 50, no. 6, pp. 3675–3684, Nov. 2014.

[123] N. K. Sheth and K. R. Rajagopal, "Optimum pole arcs for a switched reluctance motor for higher torque with reduced ripple," *IEEE Trans. Magn.*, vol. 39, no. 5, pp. 3214–3216, Sep. 2003.

[124] J. W. Lee, H. S. Kim, B. I. Kwon, and B. T. Kim, "New rotor shape design for minimum torque ripple of SRM using FEM," *IEEE Trans. Magn.*, vol. 40, no. 2, pp. 754–757, Mar. 2004.

[125] N. K. Sheth and K. R. Rajagopal, "Torque profiles of a switched reluctance motor having special pole face shapes and asymmetric stator poles," *IEEE Trans. Magn.*, vol. 40, no. 4, pp. 2035–2037, Jul. 2004.

[126] Y. K. Choi, H. S. Yoon, and C. S. Koh, "Pole-shape optimization of a switched-reluctance motor for torque ripple reduction," *IEEE Trans. Magn.*, vol. 43, no. 4, pp. 1797–1800, Apr. 2007.

[127] J. W. Jiang, B. Bilgin, and A. Emadi, "Three-phase 24/16 switched reluctance machine for a hybrid electric powertrain," *IEEE Trans. Transport. Electrific.*, vol. 3, no. 1, pp. 76–85, Mar. 2017.

[128] G. Li, J. Ojeda, S. Hlioui, E. Hoang, M. Lecrivain, and M. Gabsi, "Modification in rotor pole geometry of mutually coupled switched reluctance machine for torque ripple mitigating," *IEEE Trans. Magn.*, vol. 48, no. 6, pp. 2025–2034, Jun. 2012.

[129] C. Sahin, A. E. Amac, M. Karacor, and A. Emadi, "Reducing torque ripple of switched reluctance machines by relocation of rotor moulding clinches," *IET Electr. Power Appl.*, vol. 6, no. 9, pp. 753–760, Nov. 2012.

[130] D.-H. Lee, T. H. Pham, and J.-W. Ahn, "Design and operation characteristics of four-two pole high-speed SRM for torque ripple reduction," *IEEE Trans. Ind. Electron.*, vol. 60, no. 9, pp. 3637–3643, Sep. 2013.

[131] C. Mademlis and I. Kioskeridis, "Performance optimization in switched reluctance motor drives with online commutation angle control," *IEEE Trans. Energy Convers.*, vol. 18, no. 3, pp. 448–457, Sep. 2003.

[132] X. D. Xue, K. W. E. Cheng, J. K. Lin, Z. Zhang, K. F. Luk, T. W. Ng, and N. C. Cheung, "Optimal control method of motoring operation for SRM drives in electric vehicles," *IEEE Trans. Veh. Technol.*, vol. 59, no. 3, pp. 1191–1204, Mar. 2010.

[133] P. C. Kjaer, J. J. Gribble, and T. J. E. Miller, "High-grade control of switched reluctance machines," *IEEE Trans. Ind. Appl.*, vol. 33, no. 6, pp. 1585–1593, Dec. 1997.

[134] R. Gobbi and K. Ramar, "Optimisation techniques for a hysteresis current controller to minimise torque ripple in switched reluctance motors," *IET Electr. Power Appl.*, vol. 3, no. 5, pp. 453–460, Sep. 2009.

[135] N. T. Shaked and R. Rabinovici, "New procedures for minimizing the torque ripple in switched reluctance motors by optimizing the phase-current profile," *IEEE Trans. Magn.*, vol. 41, no. 3, pp. 1184–1192, Mar. 2005.

[136] R. Mikail, I. Husain, Y. Sozer, M. S. Islam, and T. Sebastian, "Torque-ripple minimization of switched reluctance machines through current profiling," *IEEE Trans. Ind. Appl.*, vol. 49, no. 3, pp. 1258–1267, May 2013.

[137] R. Mikail, I. Husain, M. S. Islam, Y. Sozer, and T. Sebastian, "Four-quadrant torque ripple minimization of switched reluctance machine through current profiling with mitigation of rotor eccentricity problem and sensor errors," *IEEE Trans. Ind. Appl.*, vol. 51, no. 3, pp. 2097–2104, May 2015.

[138] Z. Lin, D. Reay, B. Williams, and X. He, "High-performance current control for switched reluctance motors based on on-line estimated parameters," *IET Electr. Power Appl.*, vol. 4, no. 1, pp. 67–74, Jan. 2010.

[139] I. Husain, "Minimization of torque ripple in SRM drives," *IEEE Trans. Ind. Electron.*, vol. 49, no. 1, pp. 28–39, Aug. 2002.

[140] D.-H. Lee, J. Liang, Z.-G. Lee, and J.-W. Ahn, "A simple nonlinear logical torque sharing function for low-torque ripple SR drive," *IEEE Trans. Ind. Electron.*, vol. 56, no. 8, pp. 3021–3028, Aug. 2009.

[141] X. D. Xue, K. W. E. Cheng, and S. L. Ho, "Optimization and evaluation of torque-sharing functions for torque ripple minimization in switched reluctance motor drives," *IEEE Trans. Power Electron.*, vol. 24, no. 9, pp. 2076–2090, Sep. 2009.

[142] V. P. Vujičić, "Minimization of torque ripple and copper losses in switched reluctance drive," *IEEE Trans. Power Electron.*, vol. 27, no. 1, pp. 388–399, Jan. 2012.

[143] C. Choi, S. Kim, Y. Kim, and K. Park, "A new torque control method of a switched reluctance motor using a torque-sharing function," *IEEE Trans. Magn.*, vol. 38, no. 5, pp. 3288–3290, Sep. 2002.

[144] J. Ye, B. Bilgin, and A. Emadi, "An extended-speed low-ripple torque control of switched reluctance motor drives," *IEEE Trans. Power Electron.*, vol. 30, no. 3, pp. 1457–1470, Mar. 2015.

[145] A. D. Cheok and Y. Fukuda, "A new torque and flux control method for switched reluctance motor drives," *IEEE Trans. Power Electron.*, vol. 17, no. 4, pp. 543–557, Jul. 2002.

[146] X. Ai-De, Z. Xianchao, H. Kunlun, and C. Yuzhao, "Torque-ripple reduction of SRM using optimised voltage vector in DTC," *IET Electr. Syst. Transp.*, vol. 8, no. 1, pp. 35–43, Mar. 2018.

[147] N. Yan, X. Cao, and Z. Deng, "Direct torque control for switched reluctance motor to obtain high torque–ampere ratio," *IEEE Trans. Ind. Electron.*, vol. 66, no. 7, pp. 5144–5152, Jul. 2019.

[148] R. B. Inderka and R. W. A. A. De Doncker, "High-dynamic direct average torque control for switched reluctance drives," *IEEE Trans. Ind. Appl.*, vol. 39, no. 4, pp. 1040–1045, Jul. 2003.

[149] K. F. Wong, K. W. E. Cheng, and S. L. Ho, "On-line instantaneous torque control of a switched reluctance motor based on co-energy control," *IET Electr. Power Appl.*, vol. 3, no. 4, pp. 257–264, Jul. 2009.

[150] S. K. Sahoo, S. Dasgupta, S. K. Panda, and J.-X. Xu, "A Lyapunov function-based robust direct torque controller for a switched reluctance motor drive system," *IEEE Trans. Power Electron.*, vol. 27, no. 2, pp. 555–564, Feb. 2012.

[151] W. Ding, G. Liu, and P. Li, "A hybrid control strategy of hybrid-excitation switched reluctance motor for torque ripple reduction and constant power extension," *IEEE Trans. Ind. Electron.*, vol. 67, no. 1, pp. 38–48, Jan. 2020.

[152] T. Husain, A. Elrayyah, Y. Sozer, and I. Husain, "Dq control of switched reluctance machines," in *Proc. 28th Annu. IEEE Appl. Power Electron. Conf. Expo. (APEC)*, Mar. 2013, pp. 1537–1544.

[153] R. Abdel-Fadil and L. Szamel, "Enhancement of the switched reluctance motor performance for electric vehicles applications using predictive current control," in *Proc. Int. IEEE Conf. Workshop Óbuda Electr. Power Eng. (CANDO-EPE)*, Nov. 2018, pp. 195–200.

[154] C. Li, G. Wang, Y. Li, and A. Xu, "An improved finite-state predictive torque control for switched reluctance motor drive," *IET Electr. Power Appl.*, vol. 12, no. 1, pp. 144–151, Jan. 2018.

[155] R. Mikail, I. Husain, Y. Sozer, M. S. Islam, and T. Sebastian, "A fixed switching frequency predictive current control method for switched reluctance machines," *IEEE Trans. Ind. Appl.*, vol. 50, no. 6, pp. 3717–3726, Nov. 2014.

[156] J. Villegas, S. Vazquez, J. M. Carrasco, and I. Gil, "Model predictive control of a switched reluctance machine using discrete space vector modulation," in *Proc. IEEE Int. Symp. Ind. Electron.*, Jul. 2010, pp. 3139–3144.

[157] A. Xu, C. Shang, J. Chen, J. Zhu, and L. Han, "A new control method based on DTC and MPC to reduce torque ripple in SRM," *IEEE Access*, vol. 7, pp. 68584–68593, 2019.
[158] W. Qi, G. Zong, and H. R. Karimi, "Sliding mode control for nonlinear stochastic semi-Markov switching systems with application to SRMM," *IEEE Trans. Ind. Electron.*, vol. 67, no. 5, pp. 3955–3966, May 2020.
[159] D. T. Tran, D. X. Ba, and K. K. Ahn, "Adaptive backstepping sliding mode control for equilibrium position tracking of an electrohydraulic elastic manipulator," *IEEE Trans. Ind. Electron.*, vol. 67, no. 5, pp. 3860–3869, May 2020.
[160] N. Inanc and V. Ozbulur, "Torque ripple minimization of a switched reluctance motor by using continuous sliding mode control technique," *Electr. Power Syst. Res.*, vol. 66, no. 3, pp. 241–251, Sep. 2003.
[161] X. Sun, J. Wu, G. Lei, Y. Guo, and J. Zhu, "Torque ripple reduction of SRM drive using improved direct torque control with sliding mode controller and observer," *IEEE Trans. Ind. Electron.*, early access, Sep. 2, 2020, doi: 10.1109/TIE.2020.3020026.
[162] W. Shang, S. Zhao, Y. Shen, and Z. Qi, "A sliding mode flux-linkage controller with integral compensation for switched reluctance motor," *IEEE Trans. Magn.*, vol. 45, no. 9, pp. 3322–3328, Sep. 2009.
[163] S. K. Sahoo, S. K. Panda, and J. X. Xu, "Direct torque controller for switched reluctance motor drive using sliding mode control," in *Proc. Int. Conf. Power Electron. Drives Syst.*, vol. 2, 2005, pp. 1129–1134.
[164] M. M. N. Isfahani, S. M. Saghaian-Nejad, A. Rashidi, and H. A. Zarchi, "Passivity-based adaptive sliding mode speed control of switched reluctance motor drive considering torque ripple reduction," in *Proc. IEEE Int. Electr. Mach. Drives Conf. (IEMDC)*, May 2011, pp. 1480–1485.
[165] J. Ye, P. Malysz, and A. Emadi, "A fixed-switching-frequency integral sliding mode current controller for switched reluctance motor drives," *IEEE J. Emerg. Sel. Topics Power Electron.*, vol. 3, no. 2, pp. 381–394, Jun. 2015.
[166] S. Mir, M. E. Elbuluk, and I. Husain, "Torque-ripple minimization in switched reluctance motors using adaptive fuzzy control," *IEEE Trans. Ind. Appl.*, vol. 35, no. 2, pp. 461–468, Mar. 1999.
[167] L. O. A. P. Henriques, L. G. B. Rolim, W. I. Suemitsu, P. J. C. Branco, and J. A. Dente, "Torque ripple minimization in a switched reluctance drive by neuro-fuzzy compensation," *IEEE Trans. Magn.*, vol. 36, no. 5, pp. 3592–3594, Sep. 2000.
[168] A. R. Sadat, S. Ahmadian, and N. Vosoughi, "A novel torque ripple reduction of switched reluctance motor based on DTC-SVM method," in *Proc. IEEE Texas Power Energy Conf. (TPEC)*, Feb. 2018, pp. 1–6.
[169] J. Zhang, H. Zhang, R. Gao, and L. Wang, "Fuzzy compensation control for minimum torque ripple of switched reluctance motor system based on finite element model," in *Proc. 3rd IEEE Conf. Ind. Electron. Appl.*, Jun. 2008, pp. 2483–2486.
[170] H.-S. Ro, K.-G. Lee, J.-S. Lee, H.-G. Jeong, and K.-B. Lee, "Torque ripple minimization scheme using torque sharing function based fuzzy logic control for a switched reluctance motor," *J. Electr. Eng. Technol.*, vol. 10, no. 1, pp. 118–127, Jan. 2015.
[171] L. Kalaivani, N. S. Marimuthu, and P. Subburaj, "Intelligent control for torque-ripple minimization in switched reluctance motor," in *Proc. 1st Int. Conf. Electr. Energy Syst.*, Jan. 2011, pp. 182–186.
[172] M. Divandari and A. Dadpour, "Radial force and torque ripple optimization for acoustic noise reduction of SRM drives via fuzzy logic control," in *Proc. 9th IEEE/IAS Int. Conf. Ind. Appl. (INDUSCON)*, Nov. 2010, pp. 1–6.
[173] S. K. Sahoo, S. K. Panda, and J. X. Xu, "Iterative learning-based high-performance current controller for switched reluctance motors," *IEEE Trans. Energy Convers.*, vol. 19, no. 3, pp. 491–498, Sep. 2004.
[174] S. K. Sahoo, S. K. Panda, and J. X. Xu, "Indirect torque control of switched reluctance motors using iterative learning control," *IEEE Trans. Power Electron.*, vol. 20, no. 1, pp. 200–208, Jan. 2005.
[175] H. S. Ooi and T. C. Green, "Sensorless switched reflectance motor drive with torque ripple minimization," in *Proc. IEEE 31st Annu. Power Electron. Spec. Conf.*, vol. 3, Jun. 2000, pp. 1538–1543.
[176] D. S. Reay, T. C. Green, and B. W. Williams, "Application of associative memory neural networks to the control of a switched reluctance motor," in *Proc. 19th Annu. Conf. IEEE Ind. Electron. (IECON)*, Nov. 1993, pp. 200–206.
[177] Z. Lin, D. S. Reay, B. W. Williams, and X. He, "Torque ripple reduction in switched reluctance motor drives using B-spline neural networks," *IEEE Trans. Ind. Appl.*, vol. 42, no. 6, pp. 1445–1453, Nov. 2006.
[178] I. Takahashi and T. Noguchi, "Take a look back upon the past decade of direct torque control [of induction motors]," in *Proc. 23rd Int. Conf. Ind. Electron., Control, Instrum. (IECON)*, vol. 2, Nov. 1997, pp. 546–551.
[179] N. H. Fuengwarodsakul, M. Menne, R. B. Inderka, and R. W. Dedoncker, "High-dynamic four-quadrant switched reluctance drive based on DITC," *IEEE Trans. Ind. Appl.*, vol. 41, no. 5, pp. 1232–1242, Sep. 2005.
[180] R. B. Inderka and R. W. A. A. De Doncker, "DITC-direct instantaneous torque control of switched reluctance drives," *IEEE Trans. Ind. Appl.*, vol. 39, no. 4, pp. 1046–1051, Jul. 2003.
[181] S. Mir, M. E. Elbuluk, and I. Husain, "Torque-ripple minimization in switched reluctance motors using adaptive fuzzy control," *IEEE Trans. Ind. Appl.*, vol. 35, no. 2, pp. 461–468, Mar. 1999.
[182] S. Mir, M. S. Islam, T. Sebastian, and I. Husain, "Fault-tolerant switched reluctance motor drive using adaptive fuzzy logic controller," *IEEE Trans. Power Electron.*, vol. 19, no. 2, pp. 289–295, Mar. 2004.

ZHIKUN WANG received the B.S. degree from Guangdong Ocean University. He is currently pursuing the M.Sc. degree with the Faculty of Intelligent Manufacturing, Wuyi University.

TZE WOOD CHING (Senior Member, IEEE) received the B.Eng. and M.Sc. degrees from the Department of Electrical Engineering, Hong Kong Polytechnic University, Hung Hom, Hong Kong, and the Ph.D. degree from the Department of Electrical and Electronic Engineering, The University of Hong Kong, Pokfulam, Hong Kong, in 2002.

His current research interests include clean energy, power electronic converters, electric machines and drives, electric vehicles, and charging infrastructure. He has more than ten years of industrial experience, working with Hong Kong Electric Company and CLP Power (HK) Ltd., Hong Kong. He joined the University of Macau, Macao, China, in 2004, where he is currently an Assistant Professor with the Department of Electromechanical Engineering. He is also an Honorary Assistant Professor with the Department of Electrical and Electronic Engineering, The University of Hong Kong. He is a Chartered Engineer of the U.K., a member of the Institution of Engineering and Technology (U.K.), a member of the Chartered Institution of Building Services Engineers (U.K.), and a member of the Hong Kong Institution of Engineers. He has served as the Special Session Chair for IEEE-IECON12, IEEE-ISIE13, IEEE-ICIT15, IEEE-IEMDC15, IEEE-IECON15, EVER16, and IEEE-IEMDC2017.

SHAOJIA HUANG received the M.Sc. degree from the University of Macau. She currently works as a Lecturer with the Zhuhai College, Jilin University. Her research interests include electric vehicle and automotive engineering.

HONGTAO WANG (Member, IEEE) received the Ph.D. degree in pattern recognition and intelligent systems from the South China University of Technology in 2015.

From January 2017 to January 2019, he was a Visiting Research Fellow with the Centre for Life Sciences, National University of Singapore. He is currently a Full Professor with the Faculty of Intelligent Manufacturing, Wuyi University, and has been selected as a Thousand-Hundred-Ten Talent of Universities in Guangdong. He is also the Director of the Jiangmen Brain-like Computation and Hybrid Intelligence Research and Development Center. His current research interests include the fields of brain-like computation, pattern recognition, deep learning, and hybrid intelligence.

TAO XU received the Ph.D. degree from the Department of Biomedical Engineering, City University of Hong Kong, in 2019. He joined Wuyi University as a Distinguished Professor. His research interest includes computational neuroscience and neural prosthetic systems.